U.S. Department of Energy Reference Model Program RM2: Experimental Results

Craig Hill[1]
Vince Neary[2]
Budi Gunawan[2]
Michele Guala[1]
Fotis Sotiropoulos[1]

[1]St. Anthony Falls Laboratory, College of Science & Engineering, University of Minnesota
[2]Water Power Technologies, Sandia National Laboratories

June 24, 2014

Prepared by:
St. Anthony Falls Laboratory
College of Science & Engineering
University of Minnesota
Minneapolis, MN

Prepared for:
Wind and Water Power Technologies Program
Office of Energy Efficiency and Renewable Energy
U.S. Department of Energy
Washington, D.C.

Contents

I. Introduction

   The Reference Model Project (RMP), sponsored by the U.S. Department of Energy's (DOE) Wind and Water Power Technologies Program within the Office of Energy Efficiency & Renewable Energy (EERE), aims at expediting industry growth and efficiency by providing non-proprietary Reference Models (RM) of MHK technology designs as study objects for open-source research and development (Neary et al. 2014a,b). As part of this program, MHK turbine models were tested in a large open channel facility at the University of Minnesota's St. Anthony Falls Laboratory (UMN-SAFL). Reference Model 2 (RM2) is a 1:15 geometric scale dual-rotor cross flow vertical axis device with counter-rotating rotors, each with a rotor diameter $d_T = 0.43$m and rotor height, $h_T = 0.323$m. RM2 is a river turbine designed for a site modeled after a reach in the lower Mississippi River near Baton Rouge, Louisiana (Barone et al. 2014). Precise blade angular position and torque measurements were synchronized with three acoustic Doppler velocimeters (ADV) aligned with each rotor and the midpoint for RM2. Flow conditions for each case were controlled such that depth, $h = 1$m, and volumetric flow rate, $Q_w = 2.35$m^{3}s^{-1}, resulting in a hub height velocity of approximately $U_{hub} = 1.2$ms^{-1} and blade chord length Reynolds numbers of $Re_c = 6.1$x10^4. Vertical velocity profiles collected in the wake of each device from 1 to 10 rotor diameters are used to estimate the velocity recovery and turbulent characteristics in the wake, as well as the interaction of the counter-rotating rotor wakes. The development of this high resolution laboratory investigation provides a robust dataset that enables assessing computational fluid dynamics (CFD) models and their ability to accurately simulate turbulent inflow environments, device performance metrics, and to reproduce wake velocity deficit, recovery and higher order turbulent statistics.

II. Experimental Setup and Data Collection

   Experiments for the RM2 were completed in the Main Channel facility at the University of Minnesota's St. Anthony Falls Laboratory (SAFL). This channel is a $2.75m$ wide by $1.8m$ deep x $85m$ long channel supplied with continuous and untreated Mississippi River water. An intake gate controls the discharge level within the flume while a mechanical tailgate weir controls the flow depth and monitors flow rate. Water passes through four rows of vertically oriented baffles to break up any large scale turbulent structures before entering the test section of the channel. The RM2 model was located approximately 40m downstream of the baffles. RM2 is a 1:15 geometric scale dual-rotor cross flow vertical axis device with counter-rotating rotors, each with a rotor diameter $d_T = 0.43$m and rotor height, $h_T = 0.323$m. Various geometric and experimental hydraulic characteristics are detailed in Table 1. Schematics and photos of the experimental setup are illustrated in Figures 1 through 3. The SAFL Main Channel is equipped with a Data Acquisition (DAQ) Carriage that is capable of three-axis automated motion. This carriage was utilized during data collection to position various sensors to monitor the hydraulic environment around the RM2. Additional details of the experimental plan are discussed in Neary et al. (2012).
   Continuous discharge measurements were recorded at rates typically set to 1 Hz. Discharge was measured using a Massa M5000 ultrasonic range sensor to measure water surface elevation upstream of the tailgate weir. Discharge values are then calculated using a calibrated sharp-crested weir equation,

$$Q_{LPS} = 1838LH^{3/2}$$

where Q_{LPS} is the volumetric discharge rate in liters per second, L is the weir width ($L = 2.75$m) and H is the measured depth passing over the weir (H = water surface elevation – weir elevation).
   Velocity measurements were collected using three Nortek Vectrino acoustic Doppler velocimeters (ADVs). During performance measurements, the ADVs were positioned at hub height 3 rotor diameters ($3d_T$) upstream of the RM2 rotor location and sampled at 200Hz for 10 minutes for each rotor angular velocity. All three ADVs were synchronized with the turbine torque and angular position measurements.

Vertical velocity profiles were collected at $3d_T$ and $5d_T$ upstream of the RM2 location. Vertical point spacing was 5cm and measurements were collected at 200Hz for 3 minutes. A horizontal profile at rotor center height (i.e. hub height) was collected at $3d_T$ upstream and spanned the channel width. Wake vertical velocity profiles were collected downstream of the turbine from $1d_T$ to $10d_T$ with $1d_T$ streamwise spacing. One ADV was aligned with each of the two rotors, and the third ADV was positioned at the mid-plane between the rotors. Vertical point spacing was 2.5cm for all wake profiles, and measurements were collected for 5 minutes at each point at 200Hz. A horizontal plane was collected from $1d_T$ to $10d_T$ with $1d_T$ streamwise spacing. Cross-stream ADV point location varied, but provided enough spatial resolution to resolve key characteristics of the turbine wake. Prior to velocity measurements, the SAFL Main Channel was ponded with water and a towing test was performed to determine any rotation of the ADV measurement volume. All measurements had the resulting rotation matrix applied to the data before calculating flow statistics. Additionally, velocity timeseries measurements were despiked to remove any erroneous samples (Gunawan et al. 2011).

Torque measurements were collected from each rotor. Each rotor had an Interface Force 20Nm MRT miniature reaction torque sensor mounted in line with the rotor shaft. Voltages from the torque transducer were transmitted to the data acquisition computer via a Rotary Systems SR003 series slip ring, through an Interface Force SGA signal conditioner to convert the millivolt signal to a 0-5V range, and then acquired at the analog to digital data acquisition board. A chain drive was used to connect the shaft of each rotor to the shaft of the system speed control. A Pacific Scientific stepper motor (model K42HRFM-LEK-M2-00) controlled by a Parker Zeta 6108 indexer drive provided accurate and precise control of rotor angular velocity. Angular position was measured using a single Automation Direct rotary encoder (model TRD-SH1000-VD) mounted to the motor shaft and referenced to the counter-rotating RM2 rotor blade position. All torque and angular position measurements were synchronized with the velocity measurements.

RM2 (River Turbine)- 1:15 scale		
Parameter	SAFL Turbine Geometries	Full Scale RM2 dimensions
Blade Profile	NACA 0021	NACA 0021
Horizontal Arm Profile	NACA 0021	NACA 0021
Max Blade Chord Length	0.0267 m	0.4 m
Tip Blade Chord Length	0.016 m	0.24 m
Horizontal Arm Chord Length	0.024 m	0.36 m
Max Blade Thickness	0.0056 m	0.084 m
Tip Blade Thickness	0.0034 m	0.05 m
Horizontal Arm Thickness	0.0051 m	0.076 m
Rotor Height	0.323 m	4.84 m
Rotor Diameter	0.43 m	6.45 m
Rotor Center Height	0.677 m	>5 m
Rotor Shaft Diameter	0.0254 m	0.416 m
Solidity (= $Nc/\pi D$)	4.7%	4.7%
Blockage (= A_T/A)	10.1%	variable
Rotor Spacing	0.645 m	9.675 m
Submergence	0.323 m	4.84 m
Top tip submergence	0.163 m	2.42 m
Bottom tip submergence	0.485 m	7.26 m
Flow Depth	1.0 m	variable environment
Tip-Speed Ratios	1 to 4	1 to 6
Froude Number	0.32 (U_∞ = 1.0 m/s)	variable environment
Reynolds Number ($R_c = \lambda U_\infty L_c/\nu$)	$\approx 6.1 \times 10^4$	variable environment

Table 1: Comparison between the SAFL 1:15 RM2 turbine and the full scale design.
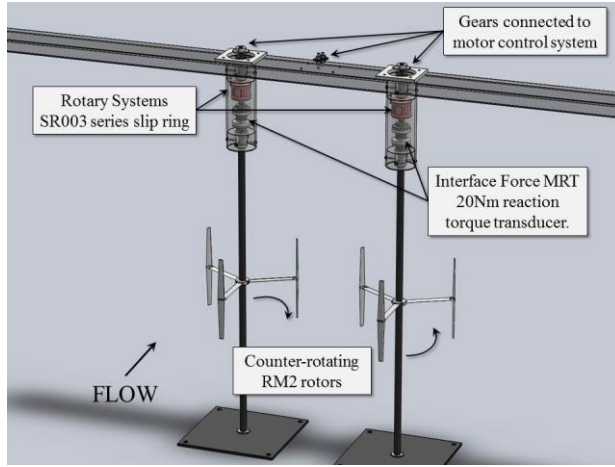
Figure 1: Instrumentation schematic of the RM2 experiment.
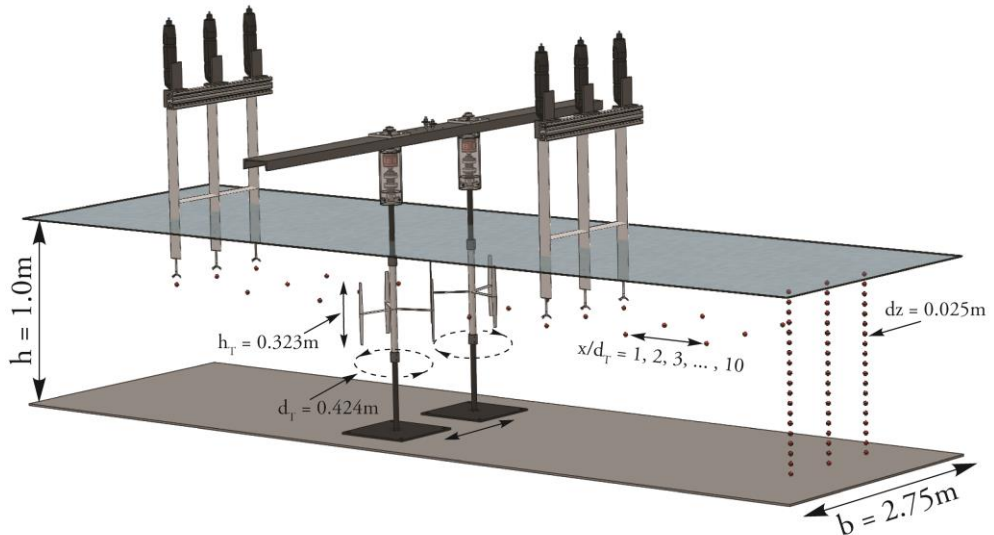
Figure 2: Schematic of the RM2 experimental setup and ADV collection locations in the SAFL Main Channel facility. Flow is from left to right.

Figure 3: Photos of the RM2 dual-rotor model in the SAFL Main Channel (left) and during torque sensor calibration (right) performed by applying known forces to the rotor and torque sensor.

III.　Data Processing

The following parameters were calculated during the processing of the velocity and turbine performance data collected during the RM2 experiments at SAFL.

a.　Mean and fluctuating velocity fields

The 200Hz velocity data output from the three Nortek Vectrino velocimeters were filtered to remove any erroneous data (see Goring and Nikora 2002; Gunawan et al. 2011). Through Reynolds decomposition, the velocity timeseries can be decomposed into the mean and fluctuation components,

$$U_i = \bar{U} + u'$$

The so calculated fluctuating velocity components are then used to calculate a number of flow statistics, which are described below.

b.　Turbulence Intensity

The turbulence intensities are dimensionless parameters that describe the level of turbulence within the flow along each spatial direction, and are defined as the root-mean squared of the fluctuating velocity component divided by the mean velocity magnitude, $\bar{U}_M = \sqrt{\bar{U}^2 + \bar{V}^2 + \bar{W}^2}$.

$$I_U = \frac{\sqrt{\overline{u'^2}}}{\bar{U}_M} \;;\quad I_V = \frac{\sqrt{\overline{v'^2}}}{\bar{U}_M} \;;\quad I_W = \frac{\sqrt{\overline{w'^2}}}{\bar{U}_M}$$

c.　Reynolds Stresses

The Reynolds stress tensor is defined as follows:

$$\tau_{ij} = \overline{u'_i u'_j}$$

when $i = j$, the results are the normal stresses ($\overline{u'u'}$, $\overline{v'v'}$, and $\overline{w'w'}$), also known as the velocity variance, and when $i \neq j$, the results are the shear stresses ($\overline{u'v'}$, $\overline{u'w'}$, and $\overline{v'w'}$).

d.　Turbulence Kinetic Energy

The turbulence kinetic energy (TKE), k, is defined as follows:

$$k = \frac{1}{2}\left(\overline{u'^2} + \overline{v'^2} + \overline{w'^2}\right)^{1/2}$$

e.　Velocity Deficit

The streamwise velocity deficit is a common metric used to report the wake velocity recovery downstream of a turbine, and is defined as follows:

$$\bar{U}_{def} = \frac{|\bar{\bar{U}}_\infty - \bar{U}_x|}{\bar{\bar{U}}_\infty}$$

where $\bar{U}_\infty$ is the upstream approach velocity at hub height, or rotor height center in the case of RM2, and $\bar{U}_x$ is the hub height velocity at position x downstream of the turbine. Here, $\bar{U}_\infty$ is measured at $x/d_T = -5$.

f.   Turbine Performance

Using the synchronous velocity, torque and rotor position measurements, various turbine parameters could be calculated. The rotor position was used to calculate the turbine angular velocity, ω. Turbine power, P_T, was calculated using the measured torque and angular velocity using,

$$P_T = \tau\omega$$

where τ is the measured torque and ω is the calculated angular velocity that was applied via the stepper motor and measured using the positional encoder integrated with the drive system. The available power within the approaching flow was calculated using the synchronous velocity measurements upstream of the RM2 location using,

$$P_A = \frac{1}{2}\rho A_T U^3$$

where P_A is the calculated available power, ρ is the density of water ($\approx 1\ kg/m^3$) dependent on water temperature (typically between 0.5°C and 1.0°C during the RM2 tests), A_T is the flow cross sectional area covered by the device ($A_T = d_T h_T$), and $\bar{U}$ is the approach flow mean velocity from the measured data using the 3 ADVs at hub height $3d_T$ upstream of the RM2. Both time-averaged turbine power ($\bar{P_T} = f(\bar{\tau})$) and available power ($\bar{P_A} = f(\bar{U})$) as well as instantaneous turbine power ($P_{T_i} = f(\tau_i)$) and available power ($P_{A_i} = f(U_i)$) were calculated. With these power calculations, the coefficient of performance, C_P, is calculated by applying the above defined values to the equation,

$$C_P = \frac{P_T}{P_A}$$

This parameter describes the fraction of power extracted from the approaching flow by the turbine. An additional dimensionless parameter used to describe the turbine performance characteristics is the tip-speed ratio, λ, defined as the ratio of the rotor tip speed to the speed of the approaching flow,

$$\lambda = \frac{\omega R}{\bar{U}}$$

Detailed performance testing characteristics for each scenario are presented in the tables in Appendix A.

IV.   Results

a.   Inflow Characteristics

Inflow velocity profiles were collected at 3 rotor diameters ($3d_T = 1.29$m) and 5 rotor diameters ($5d_T = 2.15$m) upstream of the RM2 rotor locations. The 3 ADV mount described in the Experimental Setup section was use to collect synchronous ADV measurements at these two vertical velocity profile locations. Average hub height streamwise velocity, $U_{hub} = 1.2$m/s. Turbulence intensity in the region of the RM2 rotors was approximately 5%. Summary statistics for the mean velocity ($\bar{U}$, $\bar{V}$, and $\bar{W}$), fluctuating velocities ($\sqrt{\overline{u'^2}}$, $\sqrt{\overline{v'^2}}$, and $\sqrt{\overline{w'^2}}$), turbulence intensity (I_U, I_V, and I_W), Reynolds normal

stresses ($\overline{u'u'}$, $\overline{v'v'}$, and $\overline{w'w'}$), Reynolds shear stresses ($\overline{u'v'}$, $\overline{u'w'}$, and $\overline{v'w'}$) and turbulent kinetic energy (k) are presented in Appendix B.

b. Shear Velocity

The shear velocity, u_*, in open channel flow is an important parameter in characterizing the near-wall stresses imposed by the flow on the channel boundaries. This parameter can be estimated using velocity profiles and the logarithmic law of the wall equation,

$$\frac{\overline{U}}{u_*} = \frac{1}{\kappa} \ln\left(\frac{z}{z_0}\right)$$

where $\overline{U}$ is the mean velocity at z, the distance from the wall, κ is the von Karman constant ($\kappa = 0.41$), and z_0 is the hydrodynamic roughness length. The velocity profiles measured upstream of the RM2 are plotted using this method in Figure 4. Using the method, the friction velocity, $u_* = 0.075$m/s and the resulting hydrodynamic roughness length, $z_0 = 0.001$m. Estimating the friction velocity is also possible using the Reynolds stress profile at $5d_T$ upstream (see Appendix B), which resulted in a value of $u_* = 0.054$m/s, slightly less than the law of the wall method.
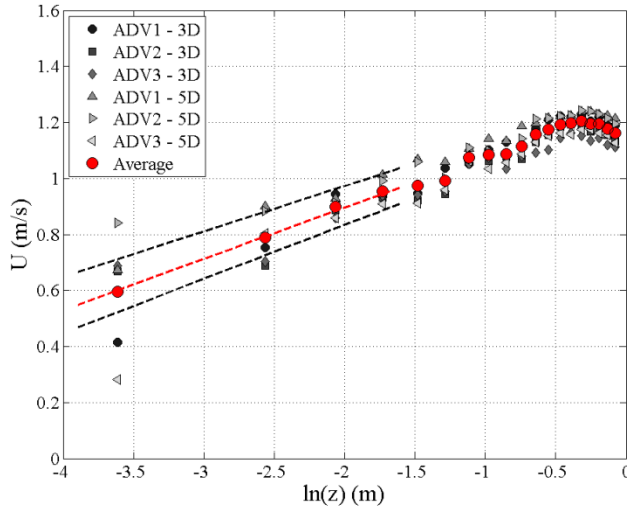
Figure 4: Plot of inflow velocity, $\overline{U}$, against the natural log of the elevation, $ln(z)$. Lower 20% of the inflow profiles used to estimate friction velocity, u_*, and hydrodynamic roughness length, z_0, using the logarithmic law of the wall equation. Red points indicate average values from the six inflow profiles collected. Red dashed line represents linear trendline against the averaged points. Black dashed lines indicated maximum and minimum linear trendlines against the data for estimating u_* and z_0.

c. Turbine Performance

Figures 5 (left rotor) and 6 (right rotor) illustrate the coefficient of power, C_P, and rotor torque as a function of angle during rotation for the RM2. Peak measured instantaneous C_P values reach 0.5 near angles $\theta \approx 15°$, 135° and 250°. When averaged, peak average C_P values are approximately 0.3 at these locations. Since the rotation angle is referenced to one of the RM2 blades, the additional two peaks correspond to the other two blades when they are in their optimal lift producing position during rotation. Performance curves for both the left and right rotors are shown in Figure 7. These plots show the coefficient of power against tip-speed ratio. Optimal performance occurred at approximately $\lambda = 2.2$ with

a corresponding $C_P = 0.05$. Performance curves were completed with the rotors in-phase, as well as by off-setting the right rotor so it lagged 30°, 60°, and 90° degrees behind the left rotor. Additionally, each rotor was tested independently to investigate effects of using dual rotors compared to a single rotor. Based on the torque sensor calibration, a scaling coefficient was applied to the measured torque values. The resulting performance curves with the scaling coefficient applied are shown in Figure 8. For this, the optimal performance occurred at approximately $\lambda = 2.2$ with a corresponding $C_P = 0.07$. Detailed performance testing characteristics for each scenario are presented in the tables in Appendix A.

The range of angles of attack for the RM2 turbine causes the blades to operate under dynamic stall. This is a Reynolds number dependent phenomenon. For the SAFL experiments, the chord Reynolds number, $Re_c \sim 10^4$, was likely below the threshold needed to properly scale stall (and lift) characteristics. For a 3-bladed cross-flow turbine of similar geometry, but different with NACA-0020 foils and a solidity $Nc/\pi D = 13.4\%$, Bachant and Wosnik (2014) reported that $Re_c \equiv \lambda U_\infty c/\nu \approx 2.1 \times 10^5$ was required to achieve Reynolds number independence.
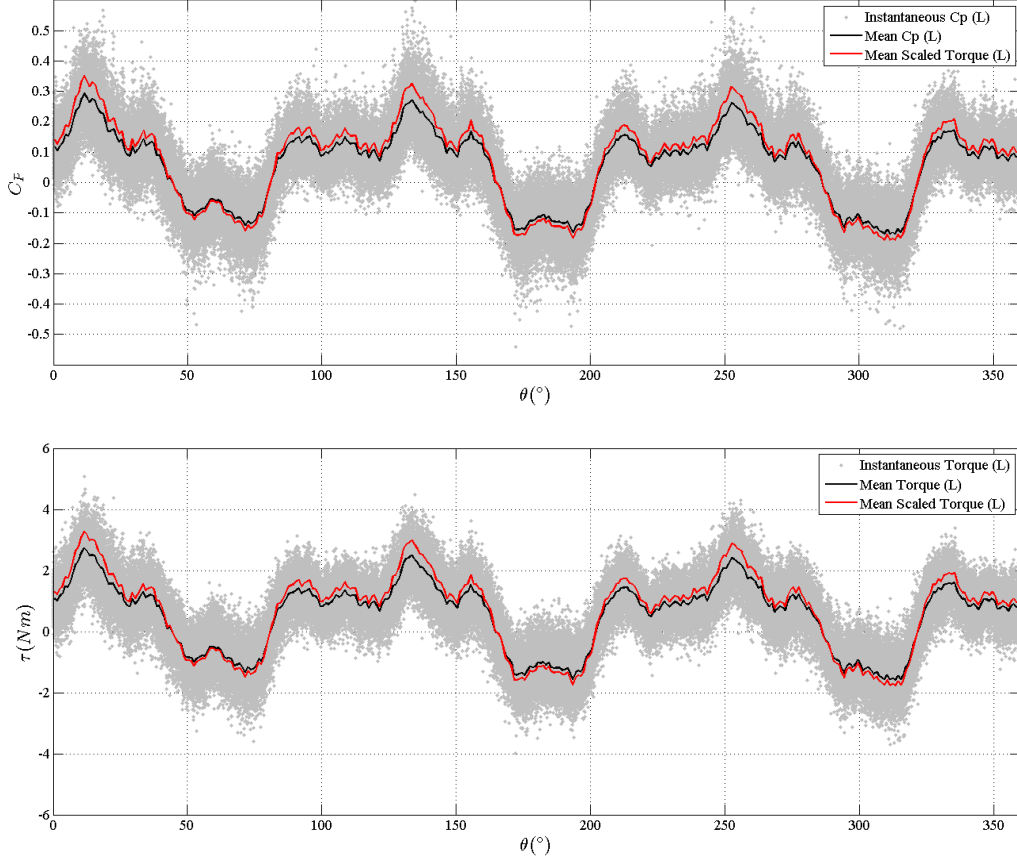
Figure 5: RM2 left rotor measured torque (bottom) and calculated C_P values (top) binned corresponding to the angle of rotation. Gray points are instantaneous torque measurements and corresponding C_P values. Solid black line shows mean torque or C_P. Solid red line shows mean torque or C_P after using scaling coefficients determined during torque sensor calibration. Measurements collected with dual-rotors in-phase and $\lambda \approx 2.2$ ($\omega = 2.0$ rps).
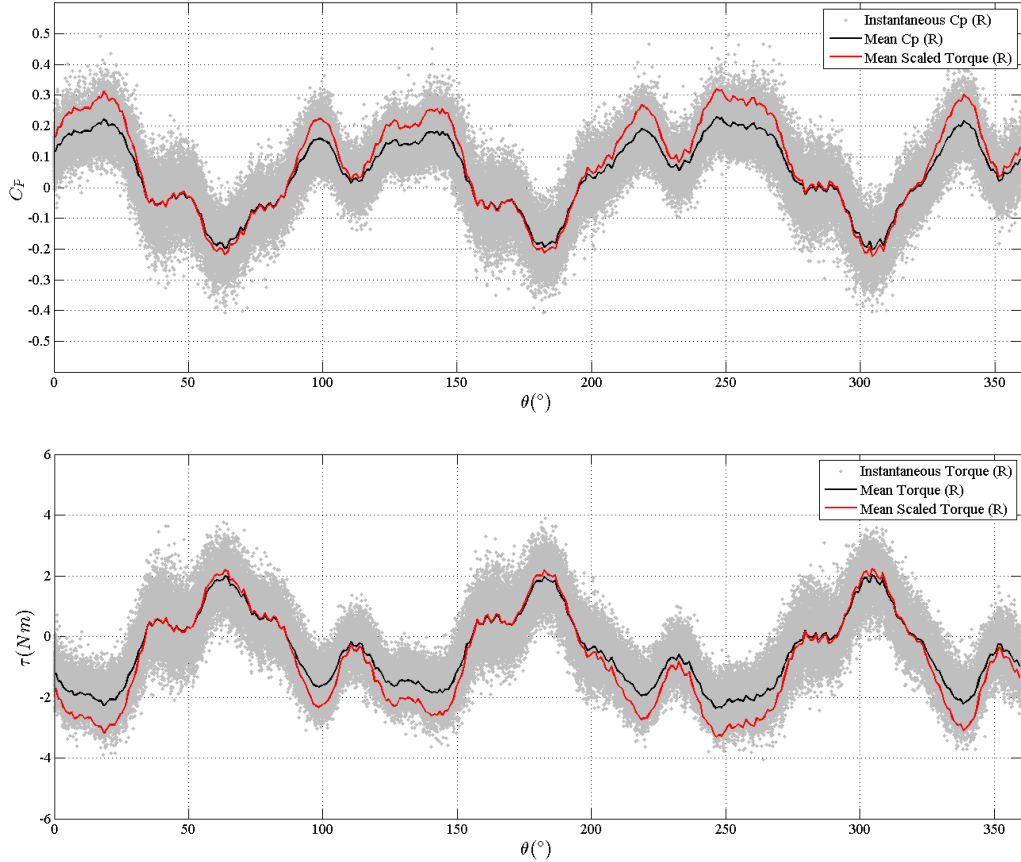
Figure 6: RM2 right rotor measured torque (bottom) and calculated C_P values (top) binned corresponding to the angle of rotation. Gray points are instantaneous torque measurements and corresponding C_P values. Solid black line shows mean torque or C_P. Solid red line shows mean torque or C_P after using scaling coefficients determined during torque sensor calibration. Measurements collected with dual-rotors in-phase and $\lambda \approx 2.2$ ($\omega = 2.0$ rps).
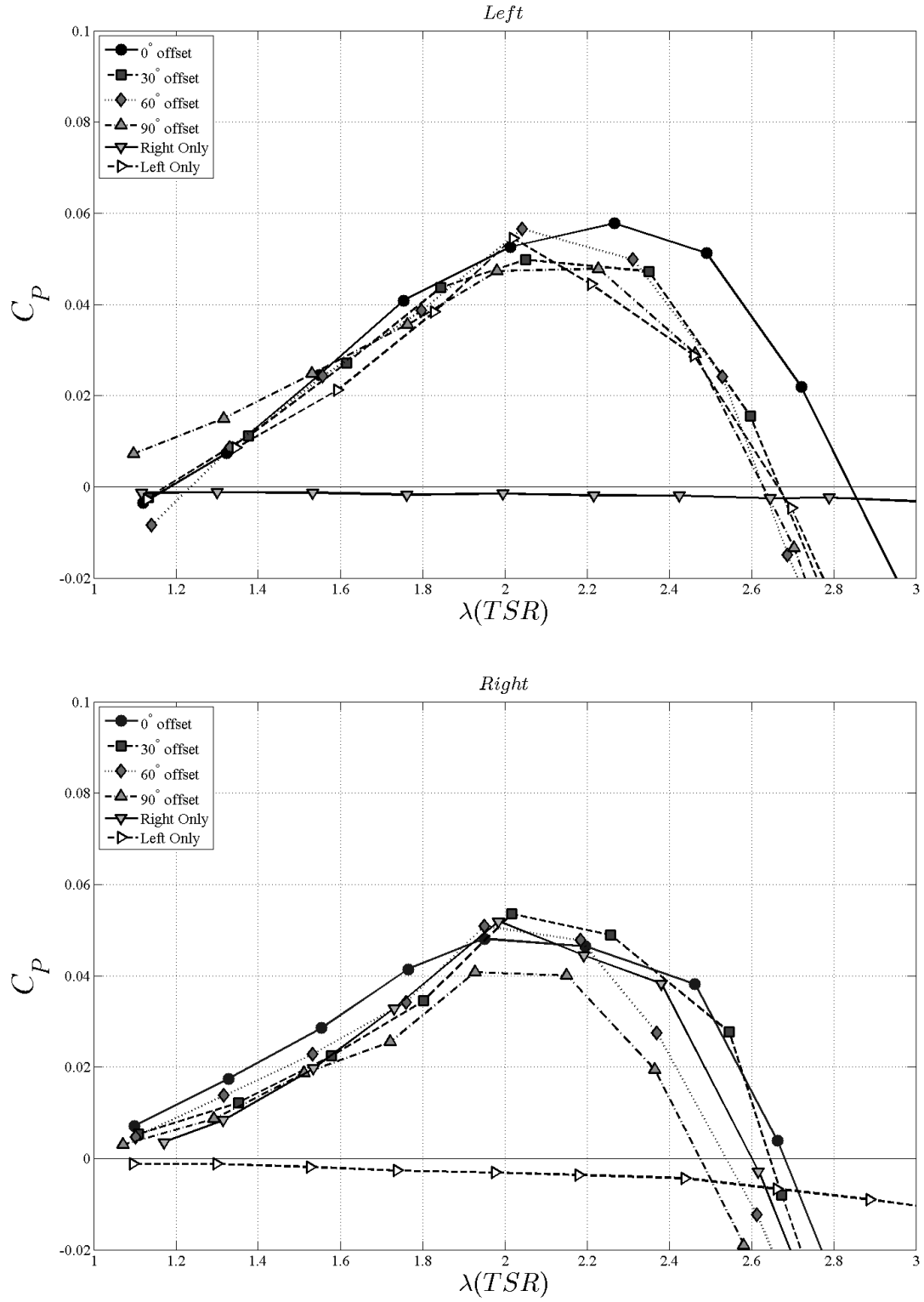
Figure 7: Calculated C_P vs. λ (coefficient of power vs. tip-speed ratio) for the left (top) and right (bottom) RM2 rotors during various rotor offset scenarios tested. Maximum C_P ($\approx$ 0.05 to 0.06) occurs near $\lambda \approx$ 2.2.
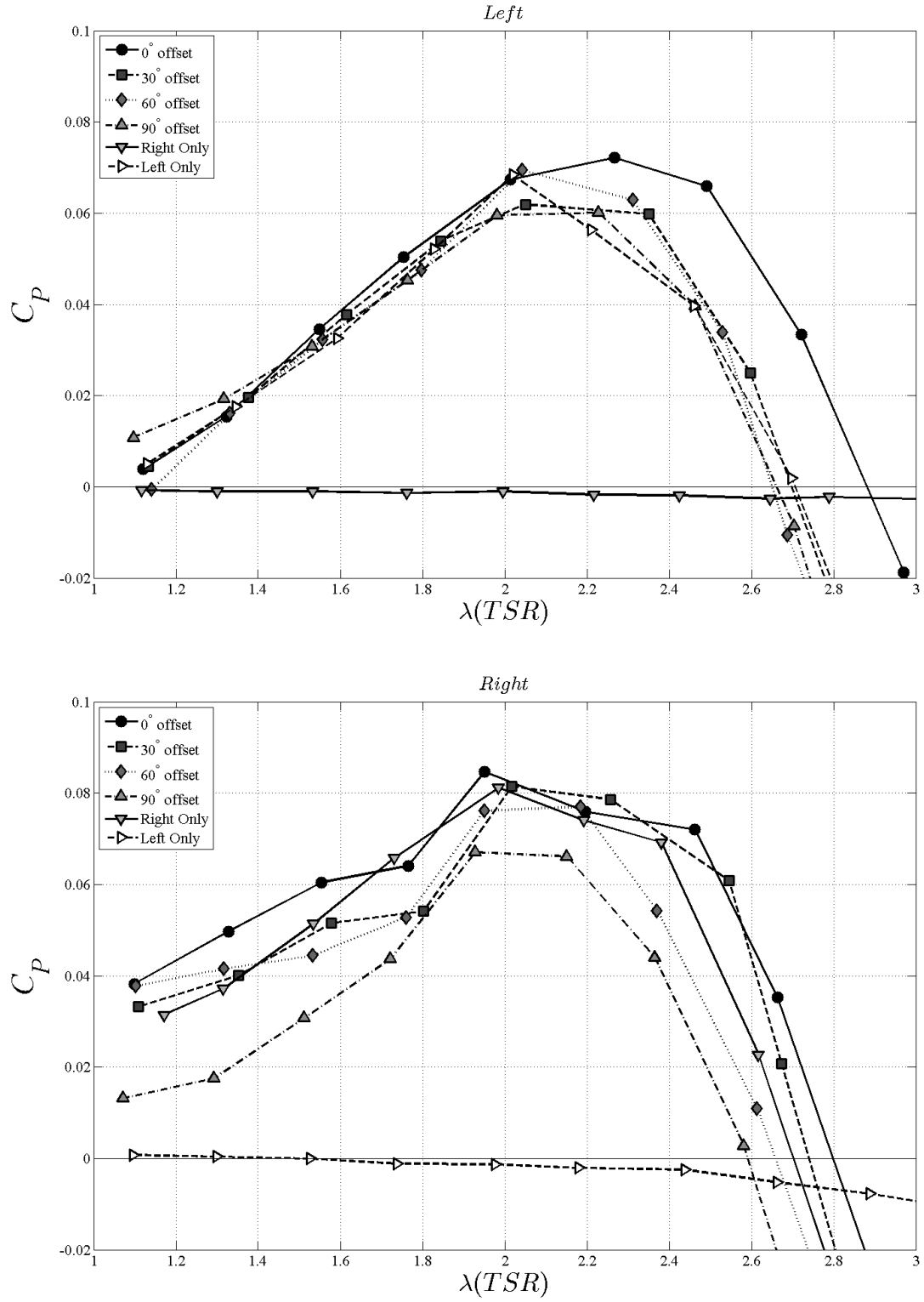
Figure 8: Scaled C_P vs. λ (coefficient of power vs. tip-speed ratio) for the left (top) and right (bottom) RM2 rotors during various rotor offset scenarios tested. Maximum C_P ($\approx$ 0.07 to 0.08) occurs near $\lambda \approx$ 2.2. Scaling done using the scaling coefficients determined from torque sensor calibration.

d. Turbine Wake Characteristics

Turbine wake velocity profiles were collected downstream of the RM2 rotor locations from $1d_T$ to $10d_T$ at $1d_T$ streamwise spacing. These data were collected along 3 vertically oriented (XZ) planes aligned with each rotor center and the mid-plane between the two rotors, as well as a horizontal (XY) plane aligned with the rotor center (i.e. hub height) (Figure 9). Contour plots for the mean streamwise velocity within the horizontal hub height plane are shown in Figure 10. Values have been normalized by the approaching flow velocity at the corresponding location upstream of the RM2 turbine. Evidence of the asymmetric wake is visible here, with the largest velocity deficit aligning with the side of the rotor that is travelling upstream. Additionally, the normalized values of turbulent kinetic energy in the horizontal plane are illustrated in Figure 11. A region of increased TKE is visible in the near wake region of each rotor. A narrow band of increased TKE stretches from the edge of each rotor aligned with the blade travelling upstream. These narrow bands extend to approximately $3d_T$ downstream of the RM2 location, at which point they merge and the elevated region of TKE expands horizontally and continues downstream until approximately $6d_T$. Similar features in the normalized mean streamwise velocity and normalized TKE are visible in the vertical planes, shown in Figures 12 and 13. The largest velocity deficit is visible up to approximately $4d_T$; however, evidence of each rotor wake extends to at least $10d_T$. The vertical plane position at the mid-plane between the two rotors illustrates where the two wakes begin to merge. This is most evident in the plots of normalized TKE, where an increase in the TKE in the mid-plane is evident between approximately $3d_T$ and $6d_T$. For additional views of the normalized streamwise velocity profiles in both the horizontal and vertical planes within the wake of the RM2, see Figure 14. It is also common to report the velocity deficit downstream of a turbine as a way to estimate the velocity recovery in the wake of the device. The streamwise velocity deficit previously defined is plotted at the RM2 rotor center height, along with streamwise root-mean squared fluctuation values and streamwise turbulence intensity, in Figure 15.
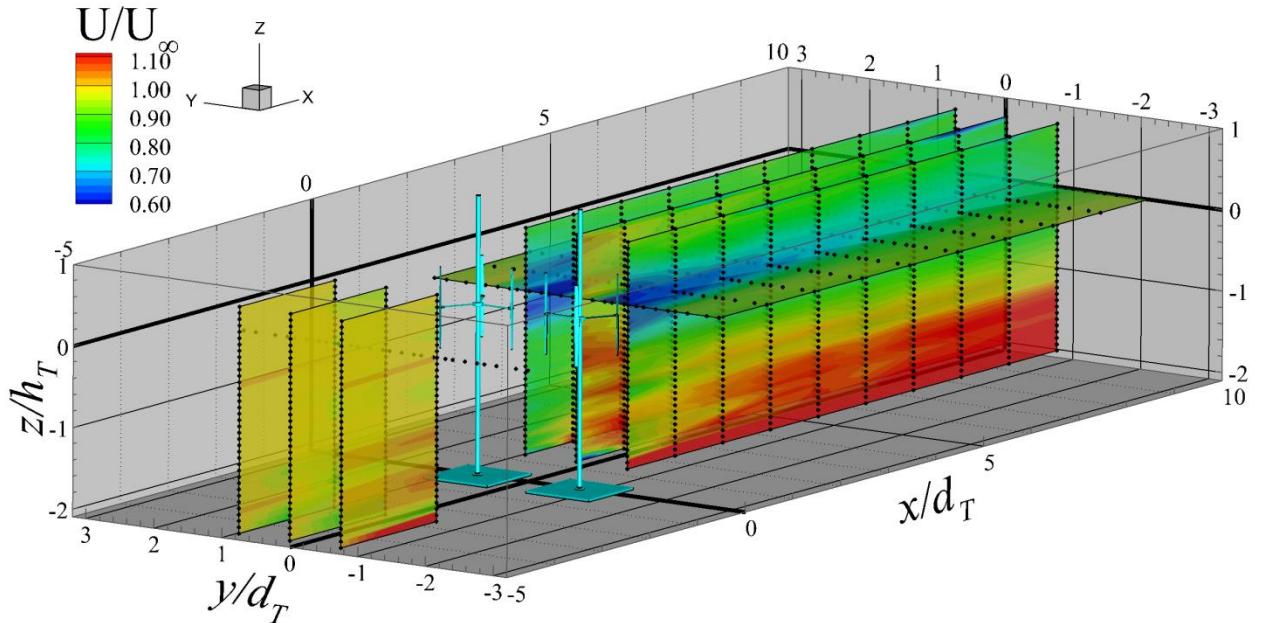
Figure 9: 3D view of the velocity data collected in the SAFL Main Channel upstream and downstream of the RM2 dual-rotor cross-flow turbine. Black circles represent ADV sampling locations used to produce contour plots of normalized streamwise velocity. RM2 model shown at $x/d_T = 0$ in light blue. Flow is left to right. Horizontal axes have been normalized by RM2 rotor diameter, $d_T = 0.43$m. Vertical axis is normalized by RM2 rotor height, $h_T = 0.323$m.

13
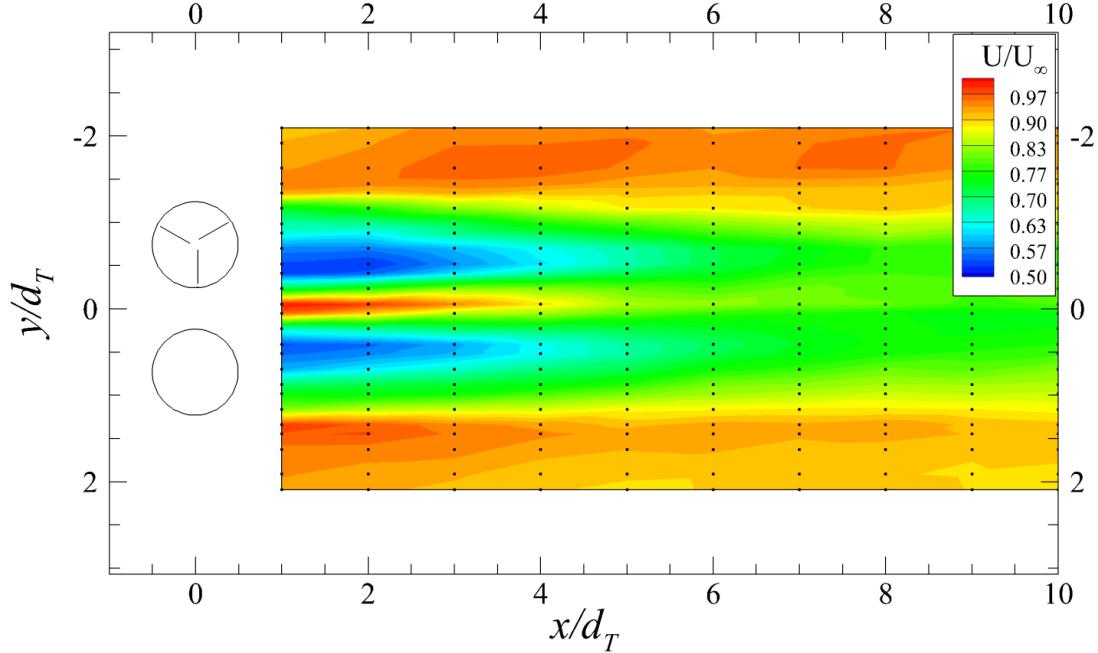
Figure 10: Normalized streamwise velocity horizontal plane (XY) contours downstream of RM2 in the SAFL Main Channel. Turbine location indicated by the two circles at $x/d_T = 0$. Vertical axis, y/h_T, shows full SAFL Main Channel width ($b = 2.75$m). Black dots indicate actual ADV measurement locations. Measurements collected with dual-rotors in-phase and $\lambda \approx 2.2$ ($\omega = 2.0$ rps). Flow is left to right.
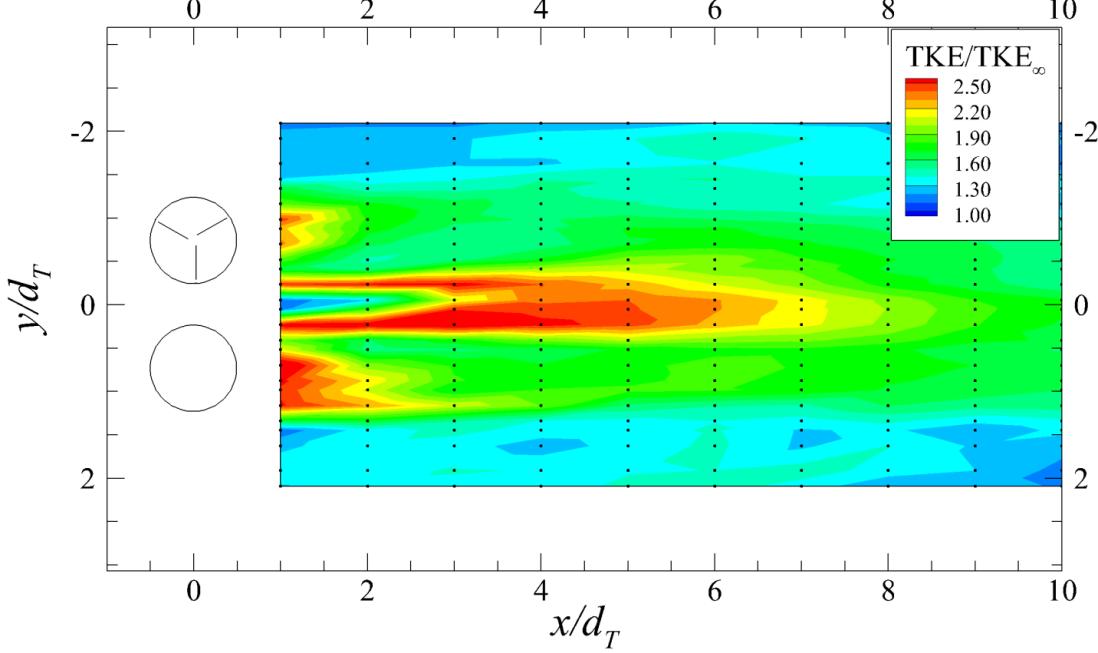

Figure 11: Normalized turbulent kinetic energy horizontal plane (XY) contours downstream of RM2 in the SAFL Main Channel. Turbine location indicated by the two circles at $x/d_T = 0$. Vertical axis, y/h_T, shows full SAFL Main Channel width ($b = 2.75$m). Black dots indicate actual ADV measurement locations. Measurements collected with dual-rotors in-phase and $\lambda \approx 2.2$ ($\omega = 2.0$ rps). Flow is left to right.
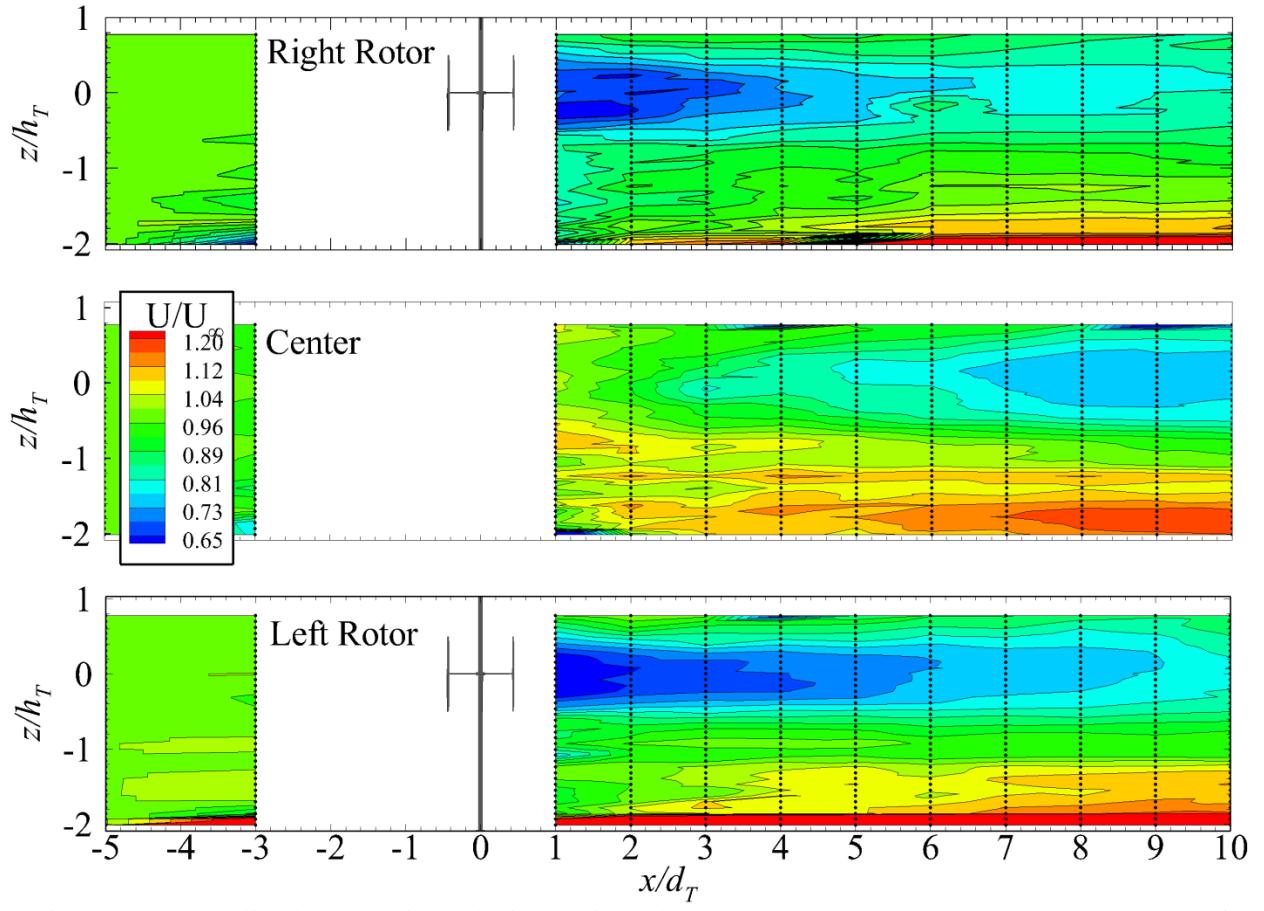
Figure 12: Normalized streamwise velocity vertical plane (XZ) contours upstream and downstream of RM2 in the SAFL Main Channel. Vertical axis, z/h_T, shows full water depth during the experiment ($h = 1.0$m). Black dots indicate actual ADV measurement locations. Measurements collected with dual-rotors in-phase and $\lambda \approx 2.2$ ($\omega = 2.0$ rps). Flow is left to right.
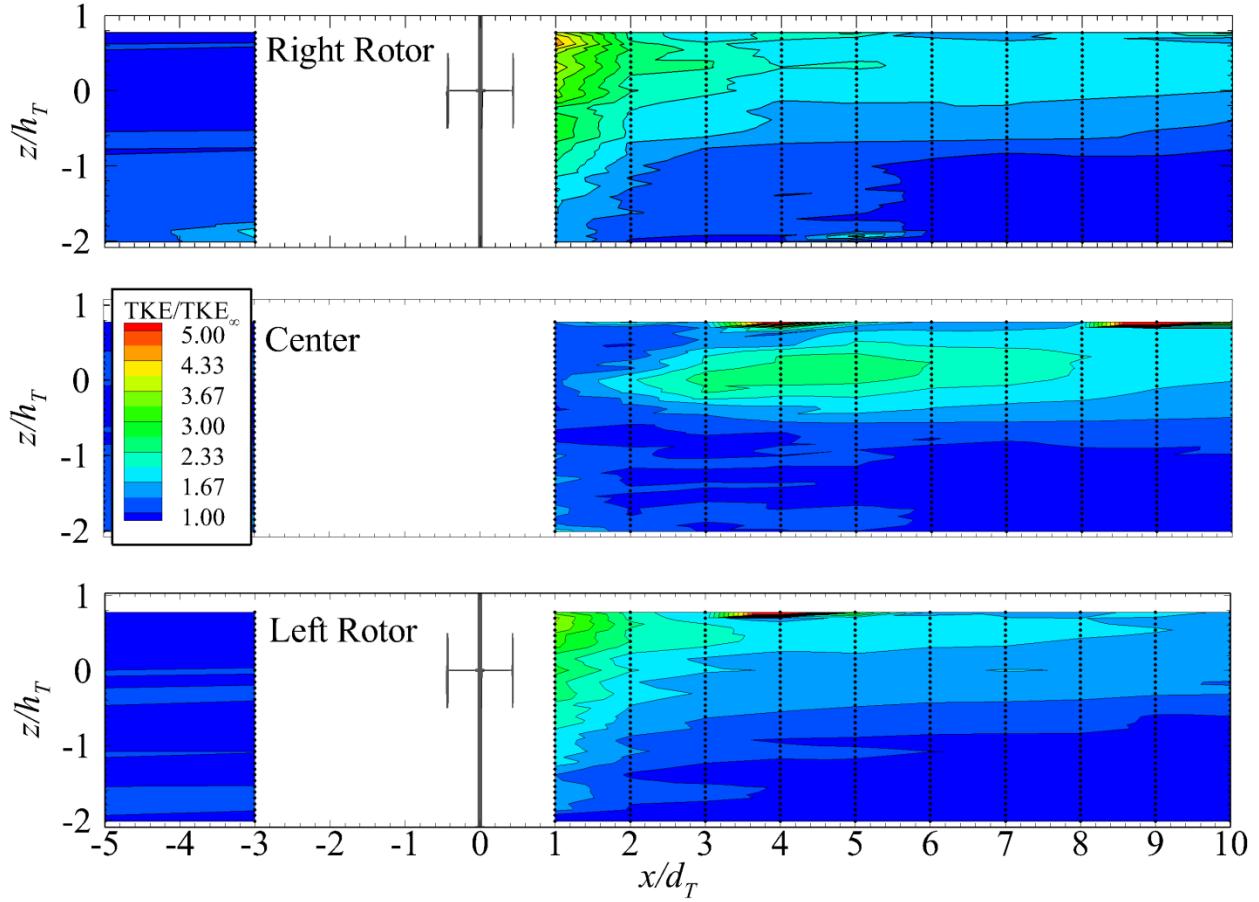
Figure 13: Normalized turbulent kinetic energy vertical plane (XZ) contours upstream and downstream of RM2 in the SAFL Main Channel. Vertical axis, z/h_T, shows full water depth during the experiment ($h = 1.0$m). Black dots indicate actual ADV measurement locations. Measurements collected with dual-rotors in-phase and $\lambda \approx 2.2$ ($\omega = 2.0$ rps). Flow is left to right.
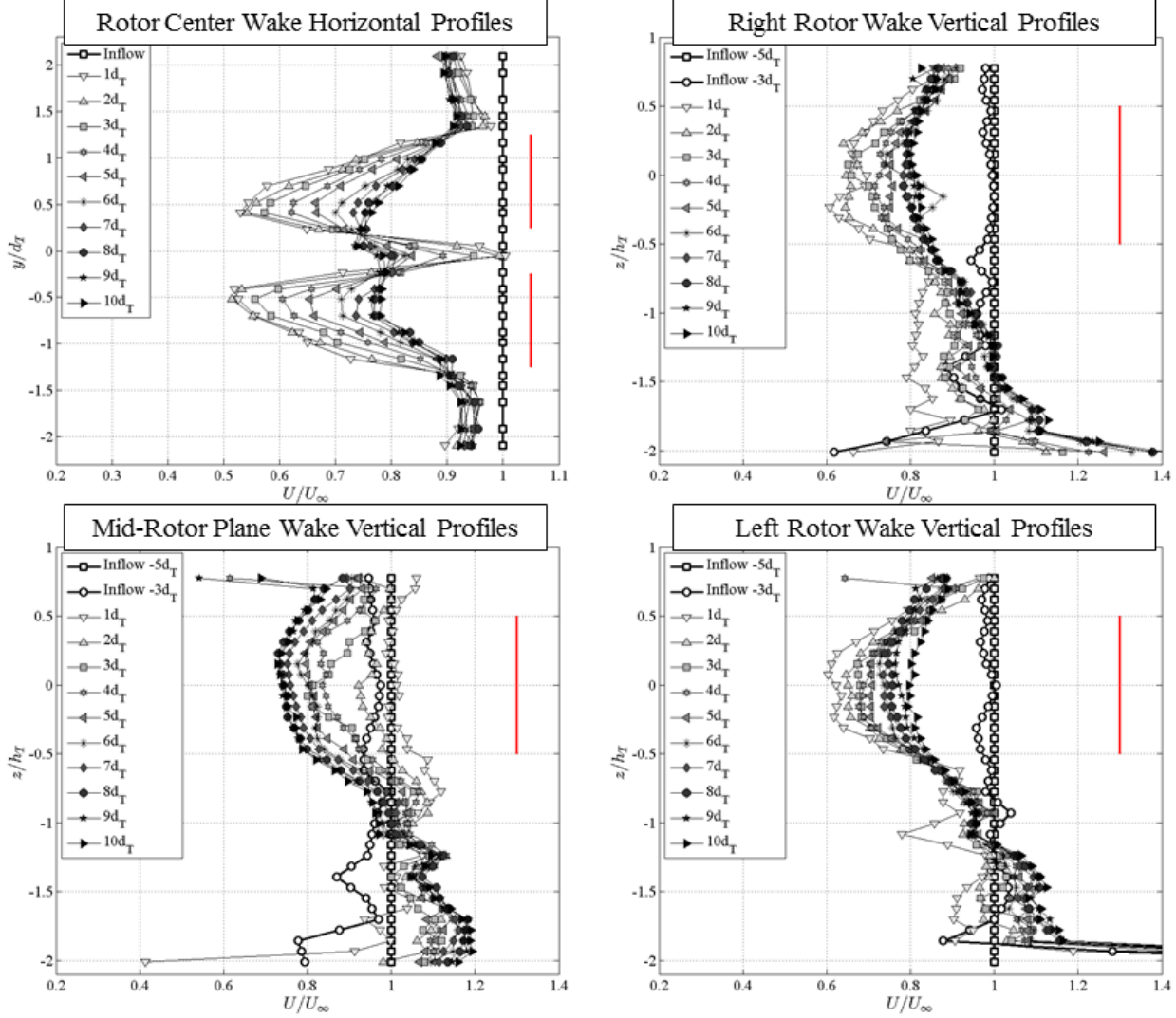
Figure 14: Normalized streamwise velocity horizontal profile in the wake of RM2. RM2 rotor height center (upper-left) and vertical profiles aligned with the center of the RM2 right rotor (upper-right), mid-rotor plane (lower-left), and RM2 left rotor (lower-right). Measurements collected with dual-rotors in-phase and $\lambda \approx 2.2$ ($\omega = 2.0$ rps). Red lines indicate horizontal or vertical span of RM2 rotor(s). All profiles have been normalized by the corresponding value from the upstream inflow profile (bold white squares equal to 1 along profile).
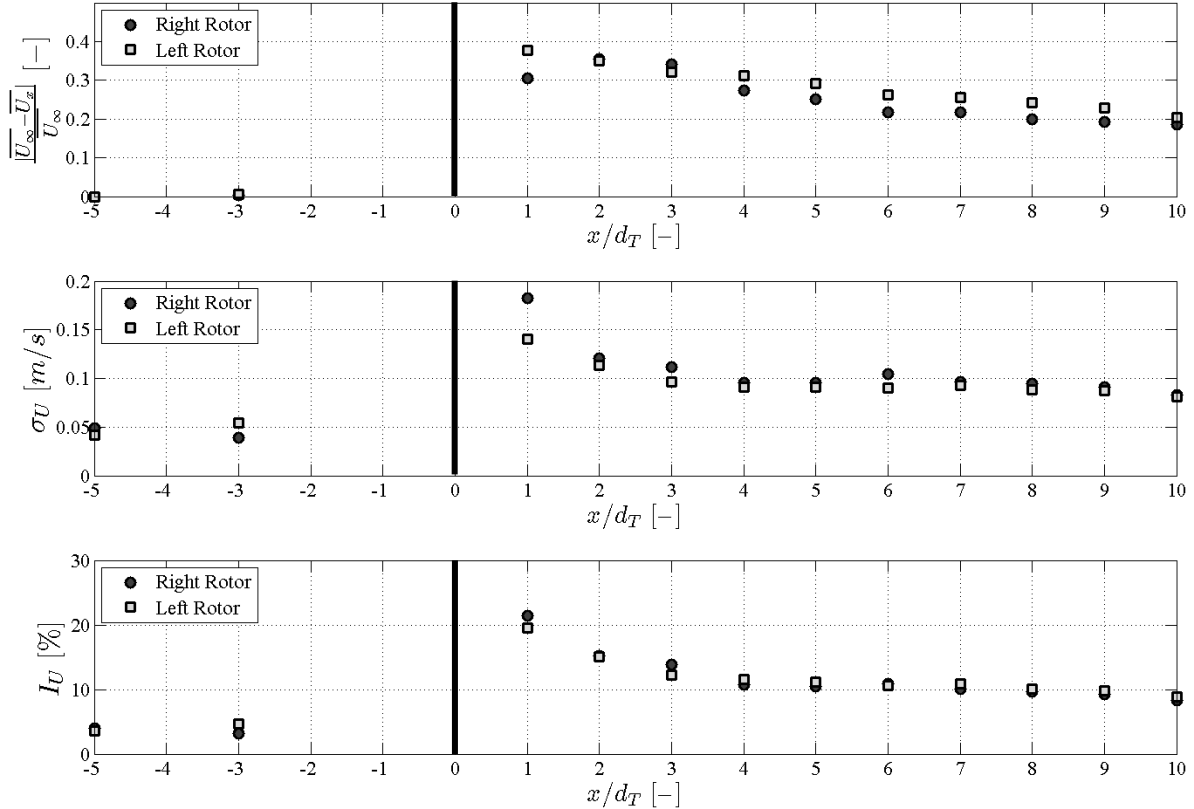
Figure 15: Rotor center height (i.e. hub height) velocity deficit (top); streamwise root-mean squared ($\sigma_U = \sqrt{\overline{u'^2}}$) (middle); and, streamwise turbulence intensity (bottom). RM2 rotors located at $x/d_T = 0$;

V.   Summary

The Reference Model 2 (RM2), a 1:15 geometrically scaled vertical axis cross-flow hydrokinetic turbine designed by the U.S. DOE for river environments was tested in the St. Anthony Falls Laboratory Main Channel facility at the University of Minnesota. Detailed performance and velocity measurements were collected to assess the interaction of RM2 with the surrounding environment. A robust dataset resulted from these experiments, providing exceptional data for CFD model validation. Performance of the dual-rotor device was found to be relatively low, possibly due to the low chord Reynolds numbers during the experiments. Maximum $C_P = 0.05$ at a tip-speed ratio of $\lambda = 2.2$. Detailed wake velocity measurements show the greatest velocity deficit extending to approximately $4d_T$ downstream of RM2, while evidence of the wake extends to $10d_T$ and beyond. At $10d_T$, the wake velocity has only recovered to approximately 80% of the upstream flow value, similar to that reported for axial flow devices (Neary et al. 2013). The lower near wake velocity deficit for RM2 compared to axial-flow decives likely is a result of the much lower performance. The interaction of the dual-rotor wakes is strongly evident between $3d_T$ and $6d_T$. Ongoing analysis and future CFD simulations will reveal more details into the interaction and structure of the dual-rotor asymmetric wake and interaction between the RM2 and a turbulent channel flow.

VI. Acknowledgment

VII. References

Bachant, P. and Wosnik, M., (2014), "Reynolds number dependence of cross-flow turbine performance and near-wake characteristics," Proceedings of the 2nd Marine Energy Technology Symposium, METS2014, April 15-18, 2014, Seattle, WA.

Barone, M., Griffith, T., and Berg, J., (2011), "Reference Model 2: Rev 0 Rotor Design," Technical Report: SAND2011-9306, Albuquerque, New Mexico: Sandia National Laboratories.

Goring, D.G. and Nikora, V.I., (2002), "Despiking acoustic Doppler velocimeter data," *J. Hydraulic Eng.*, 128(1), 117-126.

Gunawan, B., Neary, V.S., and McNutt, J., (2011), "ORNL ADV post-processing guide and MATLAB algorithms for MHK site flow and turbulence analysis," ORNL/TML-2011/338, September 2011, Prepared for the Wind and Water Power Program, Office of Energy Efficiency and Renewable Energy, U. S. Department of Energy, Washington, DC.

Neary, V.S., Hill, C., Chamorro, L.P., Gunawan, B., and Sotiropoulos, F., (2012), "Experimental Test Plan – DOE Tidal and River Reference Turbines," ORNL/TM-2012/301, August 2012. Prepared for the Wind and Water Power Program, Office of Energy Efficiency and Renewable Energy, U. S. Department of Energy, Washington, DC.

Neary, V.S., Gunawan, B., Hill, C., and Chamorro, L.P., (2013), "Near and far field flow disturbances induced by model hydrokinetic turbine: ADV and ADP comparison," *Ren. Energy*, 60, 1-6.

Neary, V.S., Previsic, M., Jepsen, R.A., Lawson, M., Yu, Y., Copping, A.E., Fontaine, A.A., Hallett, K.C., and Murray, D.K., (2014a), "Methodology for design and economic analysis of Marine Energy Conversion (MEC) technologies." SAND-2014, Sandia National Laboratories, 261 pages.

Neary, V.S., Lawson, M., Previsic, M., Copping, A., Hallett, K.C., LaBonte, A., Rieks, J., Murray, D., (2014b), "Methodology for design and economic analysis of marine energy conversion (MEC) technologies," Marine Energy Technology Symposium 2014 (METS2014), Seattle, WA, April 15-17.

VII. Appendix A: Tabulated summary of performance testing for RM2 rotors at various offsets.

Turbine Performance Characteristics – 0° offset rotors

		Turbine variables					Performance		Inflow characteristics														
	RPM	TSR (λ)	τ	bine varia	P_t	R_c	C_t	C_p	U	V	W	σ_u	σ_v	σ_w	P_a	TI (σ_u/U)	uu	vv	ww	uv	vw	uw	TKE
	RPM	-	N-m	N	N-m/s	-	-	-	m/s	m/s	m/s	m/s	m/s	m/s	N-m/s	%	m²/s²	m²/s²	m²/s²	m²/s²	m²/s²	m²/s²	m²/s²
Right Rotor	60	1.10	-0.141	n/a	0.896	2.88E+04	n/a	0.007	1.229	0.008	-0.006	0.053	0.049	0.038	129.68	4.29	2.78E-03	2.40E-03	1.44E-03	-2.30E-05	-4.00E-05	-8.30E-05	0.0813
	72	1.33	-0.294	n/a	2.189	3.46E+04	n/a	0.017	1.220	0.012	-0.013	0.050	0.053	0.044	126.65	4.09	2.49E-03	2.76E-03	1.90E-03	-9.70E-05	-1.84E-04	-4.10E-05	0.0846
	84	1.55	-0.399	n/a	3.523	4.04E+04	n/a	0.029	1.217	0.000	-0.011	0.058	0.056	0.042	125.92	4.76	3.35E-03	3.12E-03	1.79E-03	-1.29E-04	-2.58E-04	-1.32E-04	0.0909
	96	1.76	-0.519	n/a	5.223	4.61E+04	n/a	0.041	1.225	-0.005	-0.010	0.051	0.060	0.044	128.20	4.21	2.65E-03	3.59E-03	1.97E-03	-2.23E-04	-3.00E-04	-1.10E-04	0.0906
	108	1.95	-0.570	n/a	6.422	5.19E+04	n/a	0.048	1.247	-0.007	-0.015	0.046	0.049	0.038	135.14	3.68	2.10E-03	2.41E-03	1.43E-03	1.30E-05	-8.20E-05	-4.40E-05	0.0771
	120	2.20	-0.474	n/a	5.944	5.77E+04	n/a	0.046	1.230	0.000	-0.007	0.048	0.050	0.037	129.81	3.88	2.28E-03	2.47E-03	1.39E-03	-2.20E-05	-1.38E-04	-4.00E-05	0.0783
	132	2.46	-0.331	n/a	4.558	6.35E+04	n/a	0.038	1.207	0.000	-0.015	0.062	0.055	0.041	123.01	5.11	3.80E-03	3.07E-03	1.71E-03	3.60E-05	-4.40E-04	-1.47E-04	0.0927
	144	2.66	-0.033	n/a	0.483	6.92E+04	n/a	0.004	1.218	-0.001	-0.014	0.057	0.055	0.041	126.18	4.68	3.24E-03	3.06E-03	1.67E-03	8.90E-05	-4.19E-04	-1.02E-04	0.0893
	156	2.90	0.366	n/a	-6.004	7.50E+04	n/a	-0.050	1.210	0.000	-0.013	0.065	0.064	0.047	124.16	5.40	4.28E-03	4.06E-03	2.18E-03	2.48E-04	-6.62E-04	-1.04E-04	0.1026
	168	3.19	0.545	n/a	-9.617	8.08E+04	n/a	-0.083	1.188	0.009	-0.015	0.056	0.063	0.045	117.10	4.75	3.18E-03	4.02E-03	2.03E-03	1.98E-04	-3.30E-04	-1.37E-04	0.0961
	180	3.41	0.639	n/a	-12.060	8.65E+04	n/a	-0.104	1.189	0.011	-0.014	0.050	0.057	0.043	117.33	4.18	2.47E-03	3.21E-03	1.81E-03	-4.00E-06	-1.88E-04	-6.20E-05	0.0865
	192	3.62	0.463	n/a	-9.455	9.23E+04	n/a	-0.080	1.195	0.003	-0.021	0.053	0.054	0.041	119.06	4.43	2.80E-03	2.95E-03	1.66E-03	7.30E-05	-2.75E-04	-1.33E-04	0.0861
Left Rotor	60	1.12	-0.018	n/a	-0.433	2.88E+04	n/a	-0.004	1.205	0.005	0.002	0.060	0.055	0.042	122.31	5.00	3.62E-03	3.07E-03	1.73E-03	4.70E-04	-9.30E-05	-5.60E-05	0.0917
	72	1.32	0.148	n/a	0.954	3.46E+04	n/a	0.007	1.225	0.007	-0.003	0.058	0.054	0.041	128.44	4.72	3.35E-03	2.87E-03	1.65E-03	3.55E-04	-1.50E-04	3.90E-05	0.0887
	84	1.55	0.355	n/a	3.073	4.04E+04	n/a	0.025	1.220	0.003	0.001	0.053	0.054	0.041	126.81	4.33	2.79E-03	2.89E-03	1.68E-03	2.49E-04	-1.07E-04	6.00E-05	0.0858
	96	1.75	0.521	n/a	5.244	4.61E+04	n/a	0.041	1.232	-0.001	0.004	0.054	0.053	0.041	130.64	4.35	2.88E-03	2.83E-03	1.70E-03	2.65E-04	-1.82E-04	3.30E-05	0.0861
	108	2.01	0.564	n/a	6.347	5.19E+04	n/a	0.053	1.208	0.004	0.002	0.060	0.056	0.044	123.28	4.95	3.57E-03	3.16E-03	1.91E-03	3.53E-04	-2.09E-04	1.57E-04	0.0929
	120	2.27	0.532	n/a	6.690	5.77E+04	n/a	0.058	1.192	0.002	0.007	0.055	0.056	0.044	118.37	4.64	3.07E-03	3.17E-03	1.91E-03	2.34E-04	-2.18E-04	1.18E-04	0.0902
	132	2.49	0.430	n/a	5.945	6.35E+04	n/a	0.051	1.193	0.000	0.002	0.060	0.057	0.044	118.79	5.00	3.56E-03	3.20E-03	1.90E-03	2.21E-04	-3.69E-04	8.30E-05	0.0931
	144	2.72	0.169	n/a	2.545	6.92E+04	n/a	0.022	1.192	0.001	0.002	0.061	0.057	0.043	118.43	5.15	3.76E-03	3.28E-03	1.86E-03	3.32E-04	-3.17E-04	8.00E-05	0.0943
	156	2.97	-0.163	n/a	-2.657	7.50E+04	n/a	-0.023	1.183	0.000	0.000	0.049	0.063	0.047	115.46	4.11	2.36E-03	3.94E-03	2.19E-03	1.06E-04	-2.90E-04	1.82E-04	0.0921
	168	3.26	-0.380	n/a	-6.669	8.08E+04	n/a	-0.062	1.160	0.012	0.006	0.067	0.068	0.050	109.45	5.76	4.46E-03	4.59E-03	2.47E-03	1.11E-04	-4.62E-04	1.30E-04	0.1073
	180	3.48	-0.253	n/a	-4.782	8.65E+04	n/a	-0.044	1.164	0.014	0.005	0.064	0.061	0.046	110.39	5.49	4.07E-03	3.73E-03	2.09E-03	3.25E-04	-4.02E-04	6.80E-05	0.0995
	192	3.71	-0.084	n/a	-1.812	9.23E+04	n/a	-0.016	1.167	0.007	0.003	0.050	0.059	0.044	111.02	4.25	2.46E-03	3.45E-03	1.90E-03	7.90E-05	-2.02E-04	8.90E-05	0.0884

1 Thrust force (Ft) and thrust coefficients (Ct) not directly measured for RM1 and RM2 at St. Anthony Falls Laboratory, University of Minnesota.

2 R_c is the average blade chord Reynolds number $R_c = (\lambda * U * L_c) / \nu$

3 D_t = 0.43m; L_c = 0.02135m; ν = 0.000001m²/s

4 Additional summary statistics available in the corresponding folders for ADV and Performance measurements

Turbine Performance Characteristics – 30° offset rotors

		Turbine variables					Performance		Inflow characteristics														
	RPM	TSR (λ)	τ	F_t	P_t	R_c	C_t	C_p	U	V	W	σ_u	σ_v	σ_w	P_a	TI (σ_u/U)	uu	vv	ww	uv	vw	uw	TKE
	RPM	-	N-m	N	N-m/s	-	-	-	m/s	m/s	m/s	m/s	m/s	m/s	N-m/s	%	m^2/s^2	m^2/s^2	m^2/s^2	m^2/s^2	m^2/s^2	m^2/s^2	m^2/s^2
Right Rotor	60	1.11	-0.106	n/a	0.684	2.88E+04	n/a	0.005	1.218	0.013	-0.007	0.051	0.046	0.035	126.05	4.22	2.64E-03	2.10E-03	1.19E-03	5.10E-05	-9.40E-05	-2.10E-05	0.0770
	72	1.35	-0.196	n/a	1.449	3.46E+04	n/a	0.012	1.199	0.008	-0.006	0.050	0.045	0.035	120.21	4.16	2.49E-03	2.04E-03	1.23E-03	3.10E-05	-5.80E-05	-8.00E-05	0.0759
	84	1.58	-0.301	n/a	2.661	4.04E+04	n/a	0.022	1.198	-0.003	-0.012	0.042	0.047	0.037	119.77	3.53	1.79E-03	2.21E-03	1.33E-03	7.70E-05	-7.10E-05	-6.50E-05	0.0730
	96	1.80	-0.405	n/a	4.084	4.61E+04	n/a	0.034	1.199	0.001	-0.011	0.046	0.051	0.038	120.23	3.86	2.15E-03	2.60E-03	1.47E-03	4.00E-05	-1.00E-04	-1.15E-04	0.0788
	108	2.02	-0.567	n/a	6.446	5.19E+04	n/a	0.054	1.206	0.002	-0.011	0.052	0.052	0.041	122.35	4.31	2.70E-03	2.75E-03	1.67E-03	1.80E-05	-2.23E-04	-8.60E-05	0.0843
	120	2.26	-0.454	n/a	5.743	5.77E+04	n/a	0.049	1.197	0.002	-0.016	0.060	0.059	0.046	119.86	5.04	3.64E-03	3.52E-03	2.12E-03	1.92E-04	-4.44E-04	-4.20E-05	0.0963
	132	2.55	-0.210	n/a	2.983	6.35E+04	n/a	0.028	1.167	0.002	-0.009	0.076	0.065	0.047	111.83	6.48	5.73E-03	4.17E-03	2.26E-03	-6.30E-05	-8.95E-04	4.50E-05	0.1102
	144	2.67	0.072	n/a	-0.970	6.92E+04	n/a	-0.008	1.212	0.002	-0.018	0.044	0.057	0.041	124.27	3.66	1.96E-03	3.19E-03	1.68E-03	2.80E-05	-1.69E-04	-3.90E-05	0.0827
	156	2.89	0.505	n/a	-8.122	7.50E+04	n/a	-0.066	1.213	-0.002	-0.017	0.050	0.057	0.041	124.69	4.13	2.51E-03	3.23E-03	1.68E-03	1.15E-04	-2.17E-04	-2.40E-05	0.0861
	168	3.09	0.882	n/a	-15.408	8.08E+04	n/a	-0.122	1.225	-0.001	-0.012	0.051	0.051	0.037	128.16	4.17	2.61E-03	2.64E-03	1.35E-03	6.70E-05	-2.27E-04	-3.70E-05	0.0812
	180	3.35	0.889	n/a	-16.669	8.65E+04	n/a	-0.136	1.211	-0.001	-0.015	0.047	0.056	0.041	123.92	3.89	2.22E-03	3.14E-03	1.67E-03	1.27E-04	-1.83E-04	-9.40E-05	0.0838
	192	3.61	0.655	n/a	-12.968	9.23E+04	n/a	-0.110	1.196	0.002	-0.006	0.061	0.062	0.046	119.81	5.14	3.78E-03	3.85E-03	2.11E-03	3.70E-05	-4.31E-04	-9.40E-05	0.0987
Left Rotor	60	1.13	-0.004	n/a	-0.267	2.88E+04	n/a	-0.002	1.192	0.012	-0.007	0.049	0.055	0.041	118.28	4.07	2.35E-03	2.99E-03	1.69E-03	2.36E-04	-9.00E-05	-1.10E-05	0.0839
	72	1.38	0.177	n/a	1.240	3.46E+04	n/a	0.011	1.177	0.010	-0.005	0.053	0.056	0.042	113.92	4.54	2.85E-03	3.10E-03	1.80E-03	3.47E-04	-1.57E-04	3.10E-05	0.0881
	84	1.61	0.343	n/a	2.998	4.04E+04	n/a	0.027	1.171	0.002	-0.006	0.045	0.055	0.042	111.96	3.84	2.02E-03	2.97E-03	1.73E-03	1.61E-04	-7.40E-05	4.60E-05	0.0820
	96	1.84	0.479	n/a	4.829	4.61E+04	n/a	0.044	1.172	0.006	-0.006	0.049	0.059	0.047	112.27	4.20	2.42E-03	3.45E-03	2.18E-03	2.26E-04	-1.24E-04	9.50E-05	0.0897
	108	2.05	0.505	n/a	5.681	5.19E+04	n/a	0.050	1.186	0.008	-0.007	0.056	0.057	0.046	116.55	4.71	3.12E-03	3.26E-03	2.07E-03	3.87E-04	-2.47E-04	8.80E-05	0.0919
	120	2.35	0.389	n/a	4.852	5.77E+04	n/a	0.047	1.150	0.005	-0.006	0.077	0.063	0.049	106.87	6.67	5.88E-03	3.99E-03	2.40E-03	1.72E-04	-6.94E-04	1.78E-04	0.1108
	132	2.60	0.119	n/a	1.558	6.35E+04	n/a	0.015	1.144	0.003	-0.001	0.074	0.063	0.048	105.33	6.47	5.49E-03	3.96E-03	2.30E-03	4.21E-04	-7.54E-04	1.36E-04	0.1084
	144	2.82	-0.221	n/a	-3.450	6.92E+04	n/a	-0.034	1.149	0.002	-0.004	0.075	0.063	0.048	106.76	6.53	5.64E-03	3.96E-03	2.33E-03	4.74E-04	-8.65E-04	2.34E-04	0.1092
	156	3.02	-0.566	n/a	-9.371	7.50E+04	n/a	-0.087	1.164	-0.003	-0.005	0.071	0.061	0.047	110.79	6.10	5.04E-03	3.76E-03	2.19E-03	4.26E-04	-6.34E-04	1.50E-04	0.1049
	168	3.24	-0.701	n/a	-12.444	8.08E+04	n/a	-0.114	1.169	0.003	0.002	0.063	0.058	0.045	111.81	5.37	3.94E-03	3.39E-03	2.05E-03	3.79E-04	-4.08E-04	1.28E-04	0.0969
	180	3.45	-0.636	n/a	-12.095	8.65E+04	n/a	-0.109	1.174	0.004	-0.005	0.076	0.060	0.046	113.67	6.47	5.76E-03	3.55E-03	2.11E-03	4.31E-04	-6.58E-04	1.60E-04	0.1069
	192	3.65	-0.447	n/a	-9.310	9.23E+04	n/a	-0.081	1.183	0.015	-0.001	0.072	0.061	0.046	116.31	6.09	5.20E-03	3.70E-03	2.12E-03	5.12E-04	-6.94E-04	9.70E-05	0.1050

1 Thrust force (Ft) and thrust coefficients (Ct) not directly measured for RM1 and RM2 at St. Anthony Falls Laboratory, University of Minnesota.

2 R_c is the average blade chord Reynolds number $R_c = (\lambda * U * L_c) / \nu$

3 $D_t = 0.43m$; $L_c = 0.02135m$; $\nu = 0.000001 m^2/s$

4 Additional summary statistics available in the corresponding folders for ADV and Performance measurements

Turbine Performance Characteristics – 60° offset rotors

	RPM	TSR (λ)	τ	F_t	P_t	R_c	C_t	C_p	U	V	W	σ_u	σ_v	σ_w	P_a	TI (σ_u/U)	uu	vv	ww	uv	vw	uw	TKE
	RPM	-	N-m	N	N-m/s	-	-	-	m/s	m/s	m/s	m/s	m/s	m/s	N-m/s	%	m²/s²	m²/s²	m²/s²	m²/s²	m²/s²	m²/s²	m²/s²
Right Rotor	60	1.10	-0.09	n/a	0.601	2.89E+04	n/a	0.005	1.229	0.005	-0.010	0.050	0.046	0.034	129.45	4.08	2.51E-03	2.13E-03	1.19E-03	1.20E-04	2.80E-05	-3.90E-05	0.0763
	72	1.32	-0.23	n/a	1.752	3.46E+04	n/a	0.014	1.230	0.002	-0.011	0.052	0.045	0.035	129.94	4.20	2.67E-03	2.06E-03	1.21E-03	-1.30E-05	-1.01E-04	-7.00E-05	0.0771
	84	1.53	-0.33	n/a	2.944	4.04E+04	n/a	0.023	1.234	0.008	-0.002	0.044	0.052	0.041	130.83	3.53	1.90E-03	2.66E-03	1.65E-03	-3.00E-06	-6.20E-05	-1.20E-05	0.0788
	96	1.76	-0.43	n/a	4.350	4.61E+04	n/a	0.034	1.228	0.011	-0.009	0.047	0.054	0.040	129.08	3.79	2.17E-03	2.90E-03	1.58E-03	-3.00E-06	-5.00E-05	-4.40E-05	0.0815
	108	1.95	-0.60	n/a	6.774	5.19E+04	n/a	0.051	1.246	-0.003	-0.012	0.051	0.047	0.037	135.14	4.06	2.56E-03	2.25E-03	1.35E-03	-2.50E-05	-9.50E-05	-8.90E-05	0.0785
	120	2.18	-0.50	n/a	6.225	5.77E+04	n/a	0.048	1.237	0.004	-0.013	0.043	0.051	0.038	131.89	3.51	1.89E-03	2.55E-03	1.44E-03	-2.00E-06	-1.04E-04	-1.00E-05	0.0767
	132	2.37	-0.27	n/a	3.702	6.34E+04	n/a	0.027	1.253	0.007	-0.021	0.050	0.052	0.038	137.39	4.00	2.51E-03	2.69E-03	1.47E-03	1.90E-04	-1.35E-04	1.80E-05	0.0817
	144	2.61	0.10	n/a	-1.583	6.92E+04	n/a	-0.012	1.240	0.019	-0.007	0.056	0.054	0.041	133.29	4.52	3.14E-03	2.96E-03	1.64E-03	6.00E-06	-2.51E-04	-5.00E-06	0.0880
	156	2.86	0.50	n/a	-8.199	7.50E+04	n/a	-0.064	1.230	0.005	-0.017	0.050	0.059	0.043	129.87	4.08	2.52E-03	3.44E-03	1.86E-03	-2.10E-05	-2.67E-04	-1.41E-04	0.0884
	168	3.03	0.89	n/a	-15.714	8.07E+04	n/a	-0.117	1.248	0.001	-0.020	0.052	0.054	0.041	135.79	4.19	2.74E-03	2.88E-03	1.66E-03	1.17E-04	-2.02E-04	-2.80E-05	0.0853
	180	3.34	0.93	n/a	-17.514	8.65E+04	n/a	-0.142	1.215	-0.003	-0.014	0.057	0.057	0.042	125.20	4.67	3.21E-03	3.22E-03	1.80E-03	-8.00E-05	-2.74E-04	2.30E-05	0.0907
	192	3.56	0.73	n/a	-14.770	9.23E+04	n/a	-0.120	1.214	-0.001	-0.013	0.047	0.059	0.043	124.81	3.85	2.18E-03	3.43E-03	1.88E-03	1.70E-05	-1.20E-04	-2.60E-05	0.0865
Left Rotor	60	1.14	-0.08	n/a	-0.978	2.89E+04	n/a	-0.008	1.186	0.000	0.007	0.056	0.051	0.039	116.57	4.75	3.17E-03	2.56E-03	1.49E-03	3.96E-04	5.80E-05	-3.10E-05	0.0850
	72	1.33	0.16	n/a	1.049	3.46E+04	n/a	0.008	1.217	-0.004	0.003	0.057	0.052	0.040	125.90	4.70	3.26E-03	2.69E-03	1.59E-03	2.80E-04	-1.17E-04	6.00E-06	0.0868
	84	1.56	0.34	n/a	2.995	4.04E+04	n/a	0.024	1.214	0.006	-0.001	0.040	0.054	0.040	124.67	3.27	1.58E-03	2.91E-03	1.63E-03	2.04E-04	-6.10E-05	4.40E-05	0.0782
	96	1.80	0.46	n/a	4.616	4.61E+04	n/a	0.039	1.203	0.003	-0.001	0.050	0.057	0.042	121.48	4.13	2.47E-03	3.20E-03	1.79E-03	4.08E-04	-9.20E-05	3.50E-05	0.0864
	108	2.04	0.57	n/a	6.510	5.19E+04	n/a	0.057	1.190	0.005	0.003	0.064	0.060	0.048	118.09	5.34	4.05E-03	3.55E-03	2.34E-03	5.77E-04	-2.78E-04	8.10E-05	0.0997
	120	2.31	0.43	n/a	5.416	5.77E+04	n/a	0.050	1.168	0.001	0.006	0.065	0.060	0.046	111.79	5.59	4.26E-03	3.55E-03	2.15E-03	5.88E-04	-3.16E-04	1.46E-04	0.0998
	132	2.53	0.19	n/a	2.670	6.34E+04	n/a	0.024	1.175	-0.001	0.000	0.059	0.062	0.050	113.43	5.06	3.54E-03	3.88E-03	2.54E-03	4.25E-04	-1.20E-04	1.80E-04	0.0998
	144	2.69	-0.12	n/a	-1.775	6.92E+04	n/a	-0.015	1.206	0.012	0.001	0.060	0.059	0.045	122.73	4.98	3.62E-03	3.46E-03	2.04E-03	4.11E-04	-3.30E-04	6.70E-05	0.0955
	156	2.91	-0.47	n/a	-7.609	7.50E+04	n/a	-0.064	1.205	0.007	-0.001	0.062	0.059	0.046	122.56	5.12	3.82E-03	3.45E-03	2.12E-03	3.18E-04	-2.91E-04	1.50E-04	0.0969
	168	3.19	-0.64	n/a	-11.181	8.07E+04	n/a	-0.098	1.185	-0.004	0.001	0.048	0.059	0.048	116.19	4.04	2.30E-03	3.53E-03	2.26E-03	3.26E-04	-1.60E-05	1.06E-04	0.0899
	180	3.42	-0.62	n/a	-11.681	8.65E+04	n/a	-0.103	1.183	0.003	0.000	0.063	0.058	0.047	116.02	5.31	3.94E-03	3.38E-03	2.18E-03	6.81E-04	2.90E-05	1.06E-04	0.0975
	192	3.69	-0.41	n/a	-8.100	9.23E+04	n/a	-0.073	1.173	0.001	0.011	0.048	0.059	0.047	112.60	4.13	2.35E-03	3.49E-03	2.20E-03	3.37E-04	-6.60E-05	6.00E-05	0.0896

1 Thrust force (Ft) and thrust coefficients (Ct) not directly measured for RM1 and RM2 at St. Anthony Falls Laboratory, University of Minnesota.

2 R_c is the average blade chord Reynolds number $R_c = (λ*U*L_c) / v$

3 $D_t = 0.43m$; $L_c = 0.02135m$; $v = 0.000001 m^2/s$

4 Additional summary statistics available in the corresponding folders for ADV and Performance measurements

Turbine Performance Characteristics – 90° offset rotors

	RPM	TSR (λ)	τ	F_t	P_t	R_c	C_t	C_p	U	V	W	σ_u	σ_v	σ_w	P_a	TI (σ_u/U)	uu	vv	ww	uv	vw	uw	TKE
	RPM	-	N-m	N	N-m/s	-	-	-	m/s	m/s	m/s	m/s	m/s	m/s	N-m/s	%	m²/s²	m²/s²	m²/s²	m²/s²	m²/s²	m²/s²	m²/s²
Right Rotor	60	1.07	-0.06	n/a	0.402	2.88E+04	n/a	0.003	1.260	0.000	-0.020	0.071	0.058	0.043	140.26	5.65	5.06E-03	3.36E-03	1.87E-03	4.00E-06	-5.03E-04	-1.42E-04	0.1014
	72	1.29	-0.15	n/a	1.164	3.46E+04	n/a	0.009	1.254	0.000	-0.009	0.055	0.061	0.046	137.56	4.40	3.04E-03	3.72E-03	2.15E-03	2.60E-05	-2.58E-04	-1.14E-04	0.0944
	84	1.51	-0.28	n/a	2.493	4.04E+04	n/a	0.019	1.250	-0.002	-0.014	0.063	0.063	0.048	136.66	5.00	3.91E-03	4.00E-03	2.27E-03	1.34E-04	-4.63E-04	-1.40E-04	0.1009
	96	1.72	-0.34	n/a	3.454	4.61E+04	n/a	0.026	1.255	-0.013	-0.017	0.058	0.058	0.043	138.11	4.63	3.37E-03	3.40E-03	1.82E-03	3.40E-05	-3.53E-04	-3.80E-05	0.0927
	108	1.93	-0.50	n/a	5.623	5.19E+04	n/a	0.041	1.262	-0.015	-0.009	0.060	0.062	0.047	140.34	4.75	3.59E-03	3.88E-03	2.23E-03	7.60E-05	-5.07E-04	-4.80E-05	0.0985
	120	2.15	-0.43	n/a	5.448	5.77E+04	n/a	0.040	1.256	-0.006	-0.013	0.047	0.057	0.044	138.07	3.74	2.21E-03	3.25E-03	1.92E-03	6.40E-05	-2.06E-04	-6.90E-05	0.0858
	132	2.37	-0.19	n/a	2.660	6.34E+04	n/a	0.019	1.256	-0.002	-0.015	0.048	0.055	0.042	138.32	3.81	2.29E-03	3.07E-03	1.75E-03	1.11E-04	-1.76E-04	-1.23E-04	0.0843
	144	2.58	0.17	n/a	-2.599	6.92E+04	n/a	-0.019	1.256	0.003	-0.016	0.051	0.052	0.039	138.15	4.09	2.64E-03	2.70E-03	1.53E-03	1.39E-04	-2.55E-04	-6.40E-05	0.0829
	156	2.84	0.64	n/a	-10.564	7.50E+04	n/a	-0.081	1.238	-0.001	-0.017	0.052	0.054	0.040	132.54	4.17	2.67E-03	2.95E-03	1.62E-03	6.00E-05	-2.87E-04	3.80E-05	0.0851
	168	3.03	1.03	n/a	-18.083	8.07E+04	n/a	-0.135	1.249	0.006	-0.013	0.045	0.053	0.039	135.97	3.58	2.01E-03	2.82E-03	1.53E-03	-1.10E-05	-1.50E-04	-1.80E-05	0.0797
	180	3.29	1.13	n/a	-21.274	8.65E+04	n/a	-0.165	1.233	0.011	-0.014	0.055	0.052	0.039	131.08	4.44	3.00E-03	2.70E-03	1.51E-03	1.10E-04	-2.97E-04	-4.00E-05	0.0849
	192	3.53	0.96	n/a	-19.456	9.23E+04	n/a	-0.154	1.223	0.004	-0.014	0.051	0.053	0.039	127.68	4.21	2.65E-03	2.79E-03	1.56E-03	1.26E-04	-2.43E-04	-3.40E-05	0.0836
Left Rotor	60	1.10	0.15	n/a	0.910	2.88E+04	n/a	0.007	1.231	-0.013	-0.002	0.063	0.063	0.048	130.58	5.13	3.99E-03	3.94E-03	2.29E-03	3.81E-04	-4.00E-04	4.60E-05	0.1011
	72	1.32	0.25	n/a	1.906	3.46E+04	n/a	0.015	1.230	0.000	0.005	0.057	0.063	0.050	130.01	4.59	3.19E-03	3.96E-03	2.46E-03	2.38E-04	-3.53E-04	7.00E-05	0.0981
	84	1.53	0.36	n/a	3.176	4.04E+04	n/a	0.025	1.234	-0.005	-0.003	0.064	0.063	0.048	131.69	5.20	4.12E-03	3.99E-03	2.30E-03	8.20E-05	-4.29E-04	1.47E-04	0.1021
	96	1.76	0.45	n/a	4.473	4.61E+04	n/a	0.036	1.225	-0.022	0.002	0.062	0.057	0.045	128.69	5.07	3.86E-03	3.26E-03	1.99E-03	2.62E-04	-4.05E-04	8.90E-05	0.0955
	108	1.98	0.53	n/a	5.951	5.19E+04	n/a	0.047	1.227	-0.010	0.009	0.068	0.064	0.048	129.40	5.52	4.59E-03	4.10E-03	2.26E-03	2.66E-04	-5.51E-04	3.80E-05	0.1046
	120	2.23	0.46	n/a	5.791	5.77E+04	n/a	0.048	1.212	-0.002	0.005	0.070	0.062	0.048	124.94	5.73	4.83E-03	3.81E-03	2.26E-03	2.47E-04	-5.93E-04	1.11E-04	0.1044
	132	2.46	0.25	n/a	3.500	6.34E+04	n/a	0.029	1.206	-0.005	0.006	0.064	0.061	0.047	122.92	5.35	4.16E-03	3.72E-03	2.25E-03	1.74E-04	-5.37E-04	1.33E-04	0.1006
	144	2.70	-0.11	n/a	-1.565	6.92E+04	n/a	-0.013	1.199	0.002	0.007	0.057	0.059	0.046	120.59	4.77	3.28E-03	3.44E-03	2.07E-03	3.36E-04	-4.22E-04	1.18E-04	0.0938
	156	2.94	-0.52	n/a	-8.407	7.50E+04	n/a	-0.072	1.195	-0.001	0.007	0.053	0.058	0.043	119.32	4.41	2.78E-03	3.34E-03	1.88E-03	1.58E-04	-3.22E-04	2.02E-04	0.0894
	168	3.11	-0.75	n/a	-13.203	8.07E+04	n/a	-0.106	1.217	-0.027	-0.005	0.049	0.057	0.042	125.68	4.01	2.38E-03	3.28E-03	1.74E-03	1.43E-04	-2.30E-04	8.50E-05	0.0860
	180	3.37	-0.81	n/a	-15.164	8.65E+04	n/a	-0.127	1.201	0.007	-0.001	0.053	0.054	0.042	121.12	4.45	2.86E-03	2.95E-03	1.74E-03	1.96E-04	-3.07E-04	3.80E-05	0.0868
	192	3.68	-0.60	n/a	-11.903	9.23E+04	n/a	-0.107	1.173	0.000	0.004	0.063	0.059	0.044	113.11	5.34	3.92E-03	3.44E-03	1.93E-03	2.38E-04	-4.71E-04	5.00E-05	0.0964

1 Thrust force (F_t) and thrust coefficients (C_t) not directly measured for RM1 and RM2 at St. Anthony Falls Laboratory, University of Minnesota.

2 R_c is the average blade chord Reynolds number $R_c = (\lambda * U * L_c) / \nu$

3 $D_t = 0.43$m; $L_c = 0.02135$m; $\nu = 0.000001$ m²/s

4 Additional summary statistics available in the corresponding folders for ADV and Performance measurements

Turbine Performance Characteristics – Right Rotor only

	RPM	TSR (λ)	τ	Ft	Pt	Rc	Ct	Cp	U	V	W	σu	σv	σw	Pa	TI (σu/U)	uu	vv	ww	uv	vw	uw	TKE
	RPM	-	N-m	N	N-m/s	-	-	-	m/s	m/s	m/s	m/s	m/s	m/s	N-m/s	%	m²/s²	m²/s²	m²/s²	m²/s²	m²/s²	m²/s²	m²/s²
Right Rotor	60	1.17	-0.08	n/a	0.340	2.88E+04	n/a	0.004	1.153	0.021	-0.008	0.078	0.061	0.045	107.99	6.80	6.15E-03	3.73E-03	1.98E-03	-3.51E-04	-7.69E-04	-1.85E-04	0.1089
	72	1.32	-0.16	n/a	1.080	3.46E+04	n/a	0.008	1.232	0.003	-0.005	0.074	0.063	0.046	131.25	6.01	5.49E-03	4.01E-03	2.13E-03	-3.40E-04	-6.83E-04	-1.33E-04	0.1078
	84	1.53	-0.30	n/a	2.520	4.04E+04	n/a	0.020	1.232	0.004	-0.011	0.057	0.062	0.045	130.72	4.64	3.27E-03	3.90E-03	2.03E-03	-1.87E-04	-2.92E-04	-2.33E-04	0.0959
	96	1.73	-0.44	n/a	4.375	4.61E+04	n/a	0.033	1.249	0.009	-0.019	0.061	0.062	0.045	136.19	4.85	3.66E-03	3.88E-03	2.02E-03	-5.90E-05	-3.04E-04	-7.70E-05	0.0978
	108	1.99	-0.57	n/a	6.452	5.19E+04	n/a	0.052	1.225	-0.024	-0.013	0.078	0.073	0.056	129.09	6.36	6.06E-03	5.30E-03	3.14E-03	1.77E-04	-7.70E-04	-1.89E-04	0.1204
	120	2.19	-0.45	n/a	5.671	5.77E+04	n/a	0.044	1.232	0.000	-0.017	0.070	0.078	0.056	131.23	5.69	4.91E-03	6.04E-03	3.09E-03	-6.00E-06	-5.61E-04	5.10E-05	0.1185
	132	2.38	-0.37	n/a	5.093	6.35E+04	n/a	0.038	1.248	0.002	-0.017	0.057	0.059	0.044	135.92	4.56	3.24E-03	3.48E-03	1.93E-03	-1.20E-05	-3.07E-04	-1.11E-04	0.0929
	144	2.62	0.02	n/a	-0.369	6.92E+04	n/a	-0.003	1.239	0.000	-0.012	0.052	0.059	0.045	132.73	4.19	2.70E-03	3.48E-03	2.00E-03	-1.57E-04	-3.02E-04	-1.60E-05	0.0904
	156	2.85	0.43	n/a	-7.050	7.50E+04	n/a	-0.055	1.232	0.003	-0.012	0.056	0.066	0.047	130.78	4.56	3.15E-03	4.37E-03	2.22E-03	-2.72E-04	-4.03E-04	-1.07E-04	0.0987
	168	3.02	0.69	n/a	-12.059	8.08E+04	n/a	-0.089	1.252	0.017	-0.009	0.054	0.060	0.045	137.13	4.31	2.92E-03	3.57E-03	2.03E-03	-1.92E-04	-4.04E-04	4.20E-05	0.0923
	180	3.36	0.57	n/a	-10.684	8.65E+04	n/a	-0.088	1.208	0.009	-0.013	0.063	0.059	0.042	123.31	5.20	3.95E-03	3.51E-03	1.75E-03	-2.18E-04	-5.15E-04	-4.20E-05	0.0960
	192	3.59	0.21	n/a	-4.338	9.23E+04	n/a	-0.035	1.205	0.002	-0.008	0.058	0.058	0.042	122.37	4.84	3.40E-03	3.36E-03	1.75E-03	-1.90E-04	-4.33E-04	-1.14E-04	0.0922
Left Rotor	60	1.12	-0.03	n/a	-0.158	2.88E+04	n/a	-0.001	1.209	0.010	-0.003	0.050	0.056	0.040	123.41	4.15	2.52E-03	3.12E-03	1.63E-03	1.03E-04	-1.06E-04	-8.00E-06	0.0853
	72	1.30	-0.02	n/a	-0.166	3.46E+04	n/a	-0.001	1.246	0.005	0.008	0.065	0.062	0.048	135.40	5.24	4.27E-03	3.81E-03	2.29E-03	4.51E-04	-3.05E-04	8.90E-05	0.1019
	84	1.53	-0.02	n/a	-0.164	4.04E+04	n/a	-0.001	1.234	0.004	0.006	0.068	0.063	0.051	131.70	5.49	4.60E-03	3.97E-03	2.57E-03	4.30E-04	-3.65E-04	1.28E-04	0.1055
	96	1.76	-0.02	n/a	-0.215	4.61E+04	n/a	-0.002	1.226	0.001	-0.001	0.066	0.065	0.049	129.14	5.42	4.42E-03	4.23E-03	2.41E-03	3.30E-04	-4.03E-04	1.31E-04	0.1052
	108	2.00	-0.02	n/a	-0.188	5.19E+04	n/a	-0.002	1.218	-0.003	0.000	0.058	0.068	0.052	126.27	4.74	3.33E-03	4.64E-03	2.73E-03	3.10E-05	-2.39E-04	2.85E-04	0.1034
	120	2.22	-0.02	n/a	-0.225	5.77E+04	n/a	-0.002	1.219	-0.006	0.003	0.067	0.066	0.050	126.83	5.51	4.52E-03	4.37E-03	2.54E-03	3.57E-04	-4.15E-04	1.04E-04	0.1068
	132	2.43	-0.02	n/a	-0.243	6.35E+04	n/a	-0.002	1.225	-0.003	0.001	0.056	0.061	0.046	128.54	4.58	3.15E-03	3.71E-03	2.10E-03	3.08E-04	-2.12E-04	1.51E-04	0.0946
	144	2.65	-0.02	n/a	-0.324	6.92E+04	n/a	-0.003	1.225	-0.003	0.001	0.056	0.061	0.046	128.54	4.58	3.15E-03	3.71E-03	2.10E-03	3.08E-04	-2.12E-04	1.51E-04	0.0946
	156	2.79	-0.02	n/a	-0.330	7.50E+04	n/a	-0.002	1.259	0.005	0.000	0.046	0.056	0.043	139.17	3.66	2.13E-03	3.10E-03	1.89E-03	8.20E-05	-1.27E-04	4.30E-05	0.0844
	168	3.04	-0.03	n/a	-0.444	8.08E+04	n/a	-0.003	1.246	0.000	0.002	0.052	0.059	0.045	134.95	4.20	2.73E-03	3.50E-03	2.04E-03	1.57E-04	-1.88E-04	1.04E-04	0.0909
	180	3.33	-0.03	n/a	-0.496	8.65E+04	n/a	-0.004	1.218	0.008	0.003	0.066	0.058	0.045	126.50	5.45	4.40E-03	3.41E-03	1.99E-03	1.27E-04	-4.39E-04	4.30E-05	0.0990
	192	3.58	-0.02	n/a	-0.511	9.23E+04	n/a	-0.004	1.208	0.002	0.004	0.055	0.056	0.042	123.23	4.58	3.06E-03	3.13E-03	1.80E-03	1.69E-04	-1.76E-04	4.90E-05	0.0894

Column groups: Turbine variables (τ, Ft, Pt, Rc), Performance (Ct, Cp), Inflow characteristics (U … TKE).

1 Thrust force (Ft) and thrust coefficients (Ct) not directly measured for RM1 and RM2 at St. Anthony Falls Laboratory, University of Minnesota.

2 R_c is the average blade chord Reynolds number $R_c = (\lambda * U * L_c) / \nu$

3 $D_t = 0.43$m; $L_c = 0.02135$m; $\nu = 0.000001$ m²/s

4 Additional summary statistics available in the corresponding folders for ADV and Performance measurements

Turbine Performance Characteristics – Left Rotor only

Rotor	RPM	TSR (λ)	τ	Ft	Pt	Rc	Ct	Cp	U	V	W	σu	σv	σw	Pa	TI (σu/U)	uu	vv	ww	uv	vw	uw	TKE
	RPM	-	N-m	N	N-m/s	-	-	-	m/s	m/s	m/s	m/s	m/s	m/s	N-m/s	%	m^2/s^2	m^2/s^2	m^2/s^2	m^2/s^2	m^2/s^2	m^2/s^2	m^2/s^2
Right Rotor	60	1.10	0.03	n/a	-0.155	2.88E+04	n/a	-0.001	1.233	0.010	-0.013	0.055	0.055	0.040	130.94	4.49	3.07E-03	3.00E-03	1.63E-03	8.00E-06	-2.79E-04	-4.30E-05	0.0878
	72	1.30	0.02	n/a	-0.161	3.46E+04	n/a	-0.001	1.248	0.009	-0.009	0.057	0.055	0.040	135.86	4.55	3.22E-03	3.04E-03	1.60E-03	1.63E-04	-3.07E-04	-9.20E-05	0.0886
	84	1.53	0.03	n/a	-0.239	4.04E+04	n/a	-0.002	1.239	-0.002	-0.008	0.054	0.056	0.041	132.85	4.39	2.96E-03	3.14E-03	1.70E-03	1.30E-04	-2.47E-04	2.90E-05	0.0883
	96	1.74	0.04	n/a	-0.357	4.61E+04	n/a	-0.003	1.244	0.005	-0.007	0.054	0.055	0.040	134.37	4.37	2.96E-03	2.97E-03	1.62E-03	8.60E-05	-2.91E-04	-4.00E-06	0.0869
	108	1.98	0.04	n/a	-0.403	5.19E+04	n/a	-0.003	1.231	0.008	-0.009	0.056	0.054	0.040	130.17	4.52	3.09E-03	2.89E-03	1.57E-03	-9.70E-05	-2.05E-04	-8.30E-05	0.0869
	120	2.18	0.04	n/a	-0.469	5.77E+04	n/a	-0.004	1.239	0.008	-0.010	0.052	0.054	0.040	132.82	4.22	2.73E-03	2.89E-03	1.61E-03	-1.24E-04	-1.87E-04	-8.30E-05	0.0851
	132	2.44	0.04	n/a	-0.537	6.34E+04	n/a	-0.004	1.219	0.014	-0.005	0.047	0.059	0.043	126.29	3.86	2.22E-03	3.43E-03	1.87E-03	-1.43E-04	-1.28E-04	-1.18E-04	0.0867
	144	2.66	0.06	n/a	-0.829	6.92E+04	n/a	-0.007	1.218	0.002	-0.011	0.056	0.055	0.040	126.18	4.57	3.10E-03	3.02E-03	1.62E-03	-6.70E-05	-2.88E-04	-1.26E-04	0.0880
	156	2.89	0.07	n/a	-1.114	7.50E+04	n/a	-0.009	1.216	0.004	-0.012	0.055	0.054	0.040	125.64	4.55	3.06E-03	2.90E-03	1.59E-03	-1.93E-04	-1.91E-04	-6.10E-05	0.0869
	168	3.09	0.08	n/a	-1.451	8.08E+04	n/a	-0.012	1.223	-0.004	-0.008	0.052	0.054	0.040	127.81	4.27	2.73E-03	2.89E-03	1.62E-03	-1.93E-04	-1.83E-04	-1.34E-04	0.0850
	180	3.33	0.09	n/a	-1.670	8.65E+04	n/a	-0.014	1.216	-0.012	-0.008	0.048	0.052	0.039	125.40	3.92	2.27E-03	2.73E-03	1.49E-03	-7.00E-06	-1.55E-04	-9.90E-05	0.0805
	192	3.56	0.10	n/a	-2.023	9.23E+04	n/a	-0.016	1.216	0.004	-0.013	0.048	0.051	0.038	125.41	3.93	2.29E-03	2.61E-03	1.41E-03	-8.20E-05	-1.32E-04	-5.40E-05	0.0794
Left Rotor	60	1.13	-0.02	n/a	-0.350	2.88E+04	n/a	-0.003	1.195	0.003	0.007	0.063	0.057	0.043	119.55	5.24	3.93E-03	3.30E-03	1.88E-03	4.11E-04	-3.96E-04	1.28E-04	0.0954
	72	1.35	0.15	n/a	1.000	3.46E+04	n/a	0.008	1.204	0.006	0.002	0.054	0.061	0.045	121.86	4.50	2.93E-03	3.67E-03	2.06E-03	2.34E-04	-2.47E-04	1.31E-04	0.0930
	84	1.59	0.28	n/a	2.401	4.04E+04	n/a	0.021	1.187	0.002	0.007	0.065	0.060	0.045	117.15	5.45	4.19E-03	3.58E-03	1.99E-03	3.37E-04	-4.11E-04	1.65E-04	0.0988
	96	1.83	0.44	n/a	4.328	4.61E+04	n/a	0.038	1.182	0.003	0.005	0.055	0.061	0.048	115.44	4.63	2.99E-03	3.76E-03	2.29E-03	2.25E-04	-2.96E-04	1.53E-04	0.0951
	108	2.02	0.57	n/a	6.493	5.19E+04	n/a	0.055	1.204	0.006	0.003	0.060	0.056	0.042	122.09	5.01	3.64E-03	3.15E-03	1.79E-03	3.90E-04	-2.71E-04	6.50E-05	0.0926
	120	2.21	0.44	n/a	5.567	5.77E+04	n/a	0.044	1.222	0.007	0.001	0.057	0.055	0.043	127.68	4.66	3.24E-03	3.06E-03	1.85E-03	2.97E-04	-2.47E-04	8.70E-05	0.0903
	132	2.46	0.25	n/a	3.466	6.34E+04	n/a	0.029	1.208	0.011	-0.001	0.051	0.060	0.045	122.95	4.25	2.63E-03	3.59E-03	2.00E-03	1.69E-04	-2.28E-04	1.19E-04	0.0907
	144	2.70	-0.04	n/a	-0.557	6.92E+04	n/a	-0.005	1.202	0.002	0.005	0.059	0.057	0.044	121.39	4.94	3.53E-03	3.27E-03	1.93E-03	2.62E-04	-3.04E-04	7.00E-05	0.0934
	156	2.93	-0.37	n/a	-5.992	7.50E+04	n/a	-0.051	1.200	-0.001	0.003	0.060	0.055	0.042	120.76	5.01	3.61E-03	2.99E-03	1.75E-03	3.99E-04	-3.31E-04	0.00E+00	0.0914
	168	3.14	-0.40	n/a	-6.997	8.08E+04	n/a	-0.058	1.204	0.000	0.000	0.045	0.052	0.038	121.71	3.72	2.00E-03	2.72E-03	1.47E-03	1.80E-04	-1.07E-04	4.90E-05	0.0787
	180	3.42	-0.12	n/a	-2.336	8.65E+04	n/a	-0.020	1.185	-0.010	0.005	0.058	0.054	0.040	116.33	4.87	3.34E-03	2.94E-03	1.61E-03	2.82E-04	-2.91E-04	9.00E-05	0.0888
	192	3.63	0.28	n/a	5.542	9.23E+04	n/a	0.048	1.192	-0.005	-0.002	0.053	0.053	0.040	118.43	4.44	2.81E-03	2.86E-03	1.57E-03	3.38E-04	-2.19E-04	3.90E-05	0.0851

1 Thrust force (Ft) and thrust coefficients (Ct) not directly measured for RM1 and RM2 at St. Anthony Falls Laboratory, University of Minnesota.

2 R_c is the average blade chord Reynolds number $R_c = (λ*U*L_c) / ν$

3 $D_t = 0.43m$; $L_c = 0.02135m$; $ν = 0.000001 m^2/s$

4 Additional summary statistics available in the corresponding folders for ADV and Performance measurements

**VIII.** **Appendix B:** Inflow velocity characteristics for $-3d_T$ and $-5d_T$ locations.

Inflow Characteristics – $3d_T$ upstream of RM2

Inflow Characteristics $- 3d_T$ upstream of RM2

Inflow Characteristics – $5d_T$ upstream of RM2

Inflow Characteristics – $5d_T$ upstream of RM2